FAST NEUTRON TECHNIQUE FOR VOID MEASUREMENT

FAST NEUTRON SCATTERING AND ATTENUATION TECHNIQUE FOR
MEASUREMENT OF VOID FRACTIONS AND PHASE DISTRIBUTION
IN TRANSIENT FLOW BOILING

By

PETER S.L. YUEN, B.Sc.(Hons), M.Sc.

A Report (On-Campus Project)
Submitted to the School of Graduate Studies
in Partial Fulfilment of the requirements
for the Degree
Master of Engineering

McMaster University
1978

MASTER OF ENGINEERING   (1978)   McMASTER UNIVERSITY
(Engineering Physics)   Hamilton, Ontario

TITLE: Fast Neutron Scattering and Attenuation Technique
           for Measurement of Void Fractions and Phase Distribu-
           tion in Transient Flow Boiling

AUTHOR: Peter S.L. Yuen, B.Sc.(Hons)   (University of Manitoba)

                          M.Sc.   (University of Manitoba)

SUPERVISOR: Professor S. Banerjee

NUMBER OF PAGES: ix, 121

Abstract

A fast neutron scattering and transmission method
for determining void fraction and phase distribution in
transient flow boiling was investigated. Shaped aluminum test
sections containing water were placed in a fast neutron beam,
and the scattered and transmitted flux measured at several
locations. Aluminum is relatively neutron transparent and
therefore simulated the vapour phase. The aluminum pieces
were shaped to represent vapour distributions in some of the
main two-phase flow regimes (annular, inverted annular, and
stratified). The scattered flux was found to depend primarily
on the volume fraction of water (and hence void fraction) in
the test section. The transmitted flux profile on the other
hand, was sensitive to the distribution of water. The measure-
ments therefore indicated that the cross-section averaged void
fraction could be determined from the scattered flux, whereas
phase distributions could be determined from the transmitted
flux profile. These measurements were followed by a series
of experiments in which a test section containing a flowing
air-water mixture was placed in the fast neutron beam. Void
fractions determined from scattered neutron flux measurements
were compared with void fractions measured by trapping the
flowing mixture between two quick closing valves and weighing
the contents. The neutron scattering technique predicted
values in good agreement with the quick closing valve measure-
ments over the entire range of void fractions.

Acknowledgements

Table of Contents

List of Figures

List of Tables

1 INTRODUCTION AND OBJECTIVES

1.1 General Aspects

Two-phase flow through systems with complex internal geometries occur in many industrial situations. Examples are flow boiling in nuclear reactor cores and in steam generators, gas-liquid mass transfer in packed beds and fluidized bed reactors. To understand the transfer mechanisms and predict transfer rates in these systems it is often desirable to know the volume fractions of each phase at a cross-section and the phase distribution (or flow regime). In particular, void fraction (volume fraction of gas-phase) must be measured in order to interpret blowdown and emergency cooling experiments related to reactor safety assessments.

A survey of the literature reveals a rich variety of void measurement techniques. Excellent review papers on this subject have been given by Hewitt and Lovegrove (1) and Lahey (2). These techniques can be broadly grouped into the following categories: (A) volumetric, (B) electrical, (C) optical, (D) ultrasonic, and (E) radiation.

(A) Volumetric Techniques

This technique involves the direct or indirect measurement of the volume of the liquid or vapour phase within the channel.

Phase volume fractions can be measured directly by simultaneous closing quick-closing valves placed at the inlet

and exit end of the section under consideration. The valves can be closed simultaneously either by actuating a mechanical linkage system or by the using of electro-magnetically actuated systems. Examples of the use of this technique for gas-liquid and vapour-liquid flows in tubes are given in the papers of Hewitt et al (3), Roumy (4), and Serizawa (5). Schraub et al (6) have used the technique for studies in 9-rod bundles. Use of this technique has also been made on heated two-phase flows and transient measurements (7), (8).

The disadvantage of this technique is that to measure void fraction at various times during a blow-down, repeated re-establishment of the original steady-state conditions is necessary and, typically, 15 or more individual measurements are required in the first 2-3 seconds of a transient. Replication of the initial conditions for each test can be very time consuming and is clearly impossible for many situations, e.g., the Loss Of Fluid Tests (LOFT) at Idaho Falls in which an actual reactor is being blown down.

Indirect measurements of void volume depends on the fact that, in a closed circuit, the generation of voids must necessarily be accompanied by some expulsion of the liquid phase from the system. By measuring the volume expelled, one can measure the total voids generated. Applications of this method have been described by Kemp et al (9). This method gives a global average void fraction for most blowdown type experiments. It does not give information regarding void fractions in portions of the system.

Both these techniques can be inaccurate at very low or very high void fractions due to liquid sticking to piping walls.

(B) Electrical Techniques

Electrical Techniques include (i) the electrical impedance (Z) technique and (ii) the hot wire and film technique.

(i) Electrical Impedance (Z) Technique

The electrical impedance (Z) techniques can be broadly classified into those intended for measuring the global (cross sectional averaged) void fraction and those for local void fraction.

Global Z-Probe

The impedance $(\bar{Z})$ of a two-phase mixture is adequately modelled by a resistance $(\bar{R})$ in parallel with a capacitance $(\bar{C})$ so that

$$Z(f) = 1 / \sqrt{(1/\bar{R})^2 + (2\pi f\bar{C})^2} \tag{1}$$

where f is the frequency of excitation.

The capacitance $\bar{C}$ is proportional to the average dielectric constant $<\xi>$ which is related to the global void fraction $<\alpha>$ by

$$< \xi > = \xi_\ell (1 - <\alpha>) + \xi_v <\alpha> \tag{2}$$

where ξ_ℓ and ξ_v are the dielectric constants for the liquid and vapour phase respectively. Thus, using high frequency (f) excitation such that $2\pi f C \gg 1/\sqrt{R}$ (see equation 1), the capacitance

C and thus $< \xi >$ can be measured. By calibrating the probe, the global void fraction can be measured. Devices of this type have been successfully calibrated and used in out-of-core experiments (10).

These global impedance probes have the advantage that they are non-intrusive and therefore do not disturb the flow. The disadvantage of this technique includes the strong dependance of the dielectric constant of the liquid (ξ_ℓ) on temperature. As a result, a global Z-probe calibrated for one temperature may then be useless for another temperature. This would strongly limit its use in blow-down experiments in particular.

Local Z-Probe

Local Z-probes generally consist of small co-axial probes which are inserted into the flow field to measure local void fraction. When the active area of the probe (the tip) is surrounded by liquid a reading is obtained which is different from that when it is surrounded by vapour. Then the local void fraction can be determined from the time-average of a properly processed signal. The common disadvantage is that the flow may be disturbed owing to the intrusive nature of the probe. Three modes of excitation are commonly used: D.C., A.C., and R.F. excitations.

In D.C. excitation, one has more current flow when the tip is in liquid (the conducting medium) than in vapour. This technique has been extensively used in steam/water

experiments (11). In this mode of excitation, ions in the liquid phase will cause polarization unless the probe voltage is very small thus implying the processing of low level signals. Even at low voltages, electrochemical attack and deposits will age and damage the probes. Also such a technique is very sensitive to water resistivity changes, which would occur if temperature and/or water purity changes.

In A.C. excitation, a co-axial probe is driven at a fixed frequency, typically 10 kHz. A threshold is set such that when the probe is surrounded by liquid there will be a 10 kHz output signal and there will be no output when in vapour. This signal is then inverted, yielding outputs when the probe is in contact with void and no output when the probe is in liquid. The time averaged local void fraction over time T is then given by

$$\alpha = N_{void} / N_{total} \qquad (3)$$

where $N_{total} = (10 \text{ kHz})(T)$. $\qquad (4)$

Low frequency A.C. excitaton has the advantage of relatively low cost and can eliminate probe damage and polarization problems. Disadvantages include some sensitivity to liquid resistivity and the requirement of A.C. circuitry (1).

In R.F. excitation, only the dielectric constant of the two-phase fluid is sensed (see equation 1). That is, the technique is insensitive to liquid phase resistivity. A threshold is needed to discriminate between 'on' and 'off'

signals for the probe being surrounded by vapour and liquid respectively as in the case of the A.C. excitation. The main disadvantage lies in the requirement of sophisticated and expensive R.F. circuitry, apart from the disadvantage of disturbing the flow.

(ii) Hot Wire & Film Technique

The principle of operation of a hot wire or film probe is based on Joule heating and convective cooling. The probe is inserted in the medium. When it is surrounded by liquid, the heat transfer rate is higher, increasing the current flow in the probe in order to maintain a constant temperature higher than that of the ambient liquid. Likewise, the current flow decreases when the probe is surrounded by vapour. Delhaye (12) has made extensive use of conical hot film probes to study air/water flows. The main disadvantage of such a probe lies in its intrusive nature leading to disturbance of the flow medium. This leads to difficulties in interpreting the signals as discussed by Delhaye (12).

(C) Optical Techniques

Optical techniques include (i) optical local probes, (ii) infrared techniques, (iii) holographic techniques, and (iv) light attenuation techniques. The common disadvantage shared by these techniques is that it is usually not suitable for high pressure corrosive systems. However, sapphire and diamond tipped optical probes are now being developed that may make these probes more useful.

(i) <u>Local Optical Probes</u>

Optical probes are used for the measurement of local, time averaged, void fraction. The basic principle of operation of all optical probes is based on Snell's Law, i.e. a light ray, travelling from a denser medium with refractive index n_1 to a less dense medium with refractive index n_2 (i.e. $n_1 > n_2$), will be internally reflected at the interface of the two media if the angle of incidence ϕ_1 is greater than the critical incident angle ϕ_c given by

$$\phi_c = \sin^{-1} (n_1 / n_2) \tag{5}$$

The immediate result of this is that if one has a glass probe cut at 45°, and light rays enter in a coaxial fashion, the light rays will be reflected back the way they come when the tip of the probe is surrounded by air ($n = 1.0$), and will be lost in liquid ($n = 1.33$). Thus the presence of void or liquid will give rise to 'on' and 'off' light signals. Several investigators have developed fiber optics devices for the measurement of void fraction in low temperature air/water flow (13, 14).

(ii) <u>Infrared Techniques</u>

Infrared techniques have recently been used in the Marviken experiment (15). Two infrared beams with wavelengths λ_1 and λ_2 are incident on a test section. The two wavelengths are chosen such that the absorption cross-section of water is small for λ_1 and large for λ_2. The beam with λ_1 is used

as the reference beam. By Beer's Law:

$$I_{\lambda_i}(x) = I_{o\lambda_i} e^{-\mu_{\lambda_i} x} \tag{6}$$

where $I_{o\lambda_i}$ is the initial intensity at wave length λ_i , and μ_i is the corresponding macroscopic attenuation cross-section, the two beams should be differentially absorbed. It can be shown that the void fraction α is given by ($\underline{15}$):

$$\alpha = 1 - (1/\rho_\ell) C_{13} \{ \ell n(I_1/I_3) - \ell n(I_0/I_{03}) \} \tag{7}$$

where C_{13} = calibration

ρ_ℓ = density of liquid

I_i = intensity of transmitted beam

I_{o_i} = intensity of incident beam

Thus, by measuring I_1 and I_3, α can be deduced. The major disadvantage is that it can not be used in test sections with metal walls.

(iii) Holographic Techniques

Holography has recently been introduced into the field of two-phase flow by Mayinger et al ($\underline{16}$). Temperature and concentration gradients in a test section can be directly measured through the use of double exposure or two (laser) beam methods.

The principal current limitation to holographic techniques is the fact that the data can only be interpreted for two-dimensional situations.

(iv) Light Attenuation Techniques

A light beam will be attenuated when passing through

a bubbly or droplet flow. The amount of attenuation is directly proportional to the effective interfacial area. For bubbly flow, assuming the validity of Beer's law where $I/I_o = \exp(-\mu x)$, the problem reduces to determining the void dependence of the macroscopic cross section μ . Lockett et al (17) have shown that the appropriate expression for low void fractions ($\alpha < 31\%$) is given by

$$\mu = 6\alpha K / 9.21 D_b \tag{8}$$

where $\quad K = 1.08$

$\quad D_b$ = bubble diameter in metres

By measuring I/I_o, μ and thus α can be deduced. The disadvantage of this technique is that is is only reliable for low quality (bubbly) and high quality (droplet) flows, and its application to high temperature steam/water flows is difficult.

(D) <u>Ultrasonic Techniques</u>

Ultrasonic techniques include (i) Pulse-Echo, (ii) Transmission, and (iii) Doppler Shift Techniques. However, these techniques should be considered developmental and they are not suitable for high pressure steam/water systems as yet (1).

(i) <u>Pulse-Echo Technique</u>

This technique works on the Sonar principle. When an emitted ultrasonic wave reaches a vapour/liquid interface there is a large phasic impedance mismatch. This mismatch

causes a reflected signal to be returned to the transducer. The time difference between the emitted wave and the returning reflected signal yields the location of the vapour-liquid interface. This technique can easily detect bubble location and size, and appears to be a promising technique for use in either high or low quality two-phase flow (1).

(ii) Transmission Techniques

The speed of sound ($\bar{c}$) in a two-phase mixture is strongly dependent on void fraction. For example, for homogeneous flow in thermal equilibrium, the speed of sound ($\bar{c}_H$) in the mixture is given by (18):

$$1/\bar{C}_H^2 = \{\alpha \rho_v + (1-\alpha)\rho_\ell\}\{\alpha/\rho_v C_v^2 + (1-\alpha)/\rho_\ell C_\ell^2\}^* \qquad (9)$$

Similar results hold for other kinematic and thermodynamic assumptions.

By measuring the sonic velocity (1) in a two-phase mixture, it is theoretically possible to determine the void fraction α . However, the dependance of sound speed on flow structure is not as yet clearly understood.

(iii) Doppler Shift Techniques

Basically, a transmitter, installed at a fixed angle to the flow, sends out a continuous wave. Some of the energy in these wave is reflected back by the flowing material. Since the material flowing has a mean velocity component in a direction away from the reflected wave, there is a shift in apparent frequency of the scattered wave (Doppler Shift). This

---

* This assumes the flow is described by the Equal Velocities Unequal Temperature model

frequency shift can be shown to be proportional to the velo-
city of the flowing material, and by measuring the frequency
shift, one can also measure the velocity of the flow as well
as void fluctuation (1).

(E) Radiation Techniques

Radiation techniques have always been regarded as
the most reliable method of void measurement. Although they
are cumbersome to set up and use, they are generally quite
accurate. An excellent review of these techniques has been
given by Schrock (19). Radiation techniques can be further
grouped into (i) Gamma and X-ray, (ii) β-ray, and (iii)
neutron techniques.

(i) Gamma and X-ray Techniques

The attenuation of gamma rays has been extensively
applied to measure void fractions. The basic principle of
operation is the familiar Beer's Law which says that a
collimated gamma beam is exponentially attenuated by inter-
acting material in the beam path. For a single beam, it can
be shown that the void fraction α in a two-phase system is
given by (1),

$$\alpha = \ln\left[I/I(0)\right] / \ln\left[I(1)/I(0)\right] \tag{10}$$

where $I(0)$ = intensity of transmitted beam when the test
                    section is full with liquid ($\alpha = 0$)

         $I(1)$ = intensity of transmitted beam when the test
                    section is empty ($\alpha = 1$)

         I = intensity of transmitted beam for α

However, if the two-phase system is stratified and if the beam is parallel to the phases, it is then obvious that equation 10 will not hold but instead (20),

$$\alpha = [I - I(0)] / [I(1) - I(0)] \qquad (11)$$

It is then immediately clear that the application of this technique requires some knowledge of the flow regime, which is often considered a disadvantage. The other disadvantage is that gamma rays are highly attenuated by metal tube walls but to a lesser degree by water. This constitute a problem in high pressure system with low fluid to solid volume ratios.

In spite of the disadvantages mentioned, this technique has been employed in numerous investigations. Studies using it on two-phase flow in tubes include those by Bailey et al in 1955 (21) to LeVert et al in 1973 (22). Measurements in annuli are reported by Evangeliste et al (23) and Zakharova et al (24). Measurements in tube bundles are reported by Gustafsson et al (25).

The principles described above for the single beam densitometer has been extended to multiple beam arrays. Such complex devices are required for larger pipes in order to take phase distribution effects into account. Three (3)-beam gamma densitometers have been independently developed by Lassahn (26) and Heidrick et al (27). Algorithms have been developed (26, 27) with which the signals from the beams can be processed to determine void fraction and flow regime.

These algorithms are based on Beer's law and models for two-phase flow patterns.

The side-scattering of gamma-rays, has been applied to measure void fractions (28, 29), although to a much less extent. The principle of operation is based on the well-known Compton Scattering and the Klein-Nishina formula for the differential Compton Scattering cross section. A typical device consists of a collimated gamma source (Cs-137) and two NaI(Tl) detectors placed above the source and one on top of the other. The source and the two detectors are collimated so that the lines of collimation intersect at a point inside the test section where the local void fraction is to be measured. It can be shown (1) that the local average density of the two phase mixture ρ is related to the counting rates of the two detectors N_1 and N_2 by

$$\rho = \{C_2^{\beta_1} N_1^{\beta_2} / C_1^{\beta_2} N_2^{\beta_1}\} \{1 / (\beta_2 - \beta_1)\} \qquad (12)$$

where C_1, C_2, β_1, and β_2 are calibration constants. Thus, by measuring the Compton scattered gamma-rays one can measure the local average density or local void fraction.

This is a relatively new technique. It has the advantage of being non-intrusive and is promising in steady-state experiments in complex geometries. However, this technique is not suitable for transient experiments as the counting rate is extremely low. Neither is it suitable in systems where a lot of metal is present in the incident and scattered beam paths.

The attenuation of X-rays has been applied to measure chordal average void fractions. The working principle is similar to that for attenuation of gamma rays. However, X-rays are more sensitive to liquid as the attenuation cross-section increases rapidly for decreasing photon energy. Thus, Beer's law implies that these low energy X-ray beams can produce excellent phasic discrimination. An example of the application of this technique is the multi-beam X-ray system developed by Smith (30) for Edward's blowdown experiment in the U.K.

The principal disadvantage lies in its efficient absorption by metal, which makes it unsuitable for high-pressure systems.

(ii) β-ray Techniques

Absorption of β-rays may used in void fraction measurement in a manner similar to gamma rays. However, this technique has severe limitations due to the absorption of the β-rays in the channel wall. This is because β-rays are electrically charged. An example of the application of this technique is given by Perkins et al (31).

(iii) Neutron Techniques

Because neutrons are electrically neutral, they are expected to penetrate metal tube walls without much attenuation. Consequently, high pressures systems and complex geometries may be considered. Unlike gamma and X-rays, neutron beams are often more sensitive to the fluid than to metal walls. This is especially true if neutron transparent

metals like zirconium or aluminium are used with thermal neutrons, and stainless steel with fast neutrons.

The methods of void determination with neutrons can be grouped into the following categories:

(a)   attenuation of thermal neutrons by hydrogeneous materials. Thermal neutron beams from nuclear reactors have been used to determine void fractions (32, 33, 34). The basic technique relies on the exponential attenuation of the thermal neutron beam. Neutron transmission measurements were carried out in bubbly, churn and slug flows by Hancox et al (35). They used a gating technique to obtain discrete transmission measurements over time-intervals much smaller than the dominant void fluctuation period. This technique utilizing thermal neutrons is limited to relatively thin test sections.

(b)   thermalization of fast neutrons by hydrogeneous material. This technique is based on the phenomenon that fast neutrons, on passing through materials of high scattering cross-section (or moderating power), are slowed down to thermal energies. The fractional loss in energy when a neutron collides with an atom is greatest for the hydrogen atom. Therefore, by passing a beam of fast neutrons through a series of materials of varying hydrogen density, a relation-ship should be observed between hydrogen content and measured thermal neutron intensity. However, the complexity of neutron moderation theory does not lend itself as readily to a simple

mathematical treatment as does thermal neutron transmission.
Thus, in this technique, the usual experimental approach is
to prepare a standard calibration curve from samples of known
hydrogeneous material content and to relate the measured
thermal neutron intensity of an unknown sample to this curve.
This technique has been applied in moisture determination
with californium sources (36) and in steam volume fraction
determination in a pipe with 14 MeV neutrons (37).

(c)   combined moderation and attenuation of fast neutrons
by hydrogeneous materials containing strong absorbers of
thermal neutrons. In a strong thermal neutron absorber, the
thermal flux is directly related to the moderation of the
fast flux in the immediate vicinity. Sha and Bonilla (38)
performed an Out-of-Pile experiment employing this technique
to determine void fractions. Fast neutrons from a Sb-Be
neutron source were used and Boron was dissolved in a 76-203 mm
diameter pipe to increase the attenuation coefficient of the
water in the pipe. Optimum application of this technique
requires test sections larger than 25 mm.

From the above discussions, it is evident that in
experiments where the test section is thick walled, fast
neutron techniques are preferable. Scattering of fast neutron,
a relatively new technique, has already been used to measure
void fractions for two-phase flow in pipes. Preliminary work
was reported by Rousseau (39) and Banerjee (40). These
investigations indicated that the technique was promising.

However, no systematic direct calibration was done.

1.2   Objectives

The present work was undertaken to increase confidence in the fast neutron scattering technique introduced by Rousseau (39) and Banerjee (40). It is meant to be the first of a series of series of efforts in an extensive calibration program for void fraction in air-water flow through pipes and other geometries such as rod bundles and packed beds. Test-sections 25.4 mm and 50.8 mm in diameter were used in the work reported here. Aluminum specimens of uniform cross-sections were inserted into the test section to simulate air (void) such that the major flow patterns of annular, inverted annular, and stratified flows were obtained.

A collimated horizontal fast-epithermal neutron beam of rectangular cross-section, 50 mm wide and 10 mm high, was made incident on the test-section whose axis was vertical. The scattered and transmitted flux was counted. The scattered and subsequently thermalized neutrons were counted by a neutron counter placed at 90° to the beam in the plane of the beam.

The scattered thermal flux was expected, to a first approximation, to depend on the mass of hydrogeneous material at the cross-section and not on its distribution. This is because several collisions are required to downscatter the neutrons into the thermal region. At the thermal level, neutron scattering is characterized by a diffusion cross-section of about $3.4 \ cm^{-1}$ corresponding to a mean free

path of 3 mm which is much less than the test section dimension
(50 mm). The test section diameter is itself much less than the
mean free path of absorption which is about 450 mm. Hence,
the incident fast/epithermal neutron should have, on the
average, undergone a large number of collisions in the water
before leaving the water and being counted as thermal neutrons.
Under these conditions, the water in the test section behaves
like an isotropic source of thermal neutrons and the counted
scattered flux conveys information regarding the amount, but
not the distribution of water in the test section.

On the other hand, the transmitted flux may be counted
with collimated detectors. This gives a measure of the amount
of water in the detector's collimation zone since different
water path lengths will result in attenuation of the neutrons
to different extents (approximately exponential). Thus, by
counting the transmitted neutron flux at several locations,
the distribution of hydrogeneous material may be reconstructed
to the extent that the main two-phase flow regime can be
identified.

The main objectives of the present work can then be
listed as:

(a)   to determine whether the scattered thermalized neutron
flux is related to the amount of hydrogeneous material and
hence void fraction at a cross-section;

(b)   to determine whether the scattered flux depends on
the distribution of the hydrogeneous material, and if so, to

what extent;

(c)   to determine whether the measurement of transmitted flux can be used to identify the main flow regimes.

2 EXPERIMENTAL SET-UP

In this section, the experimental facilities and set-up, whether existing or specially built, are described.

2.1 McMaster Nuclear Reactor (MNR)

The McMaster Nuclear Reactor is located in the Reactor Building. This reactor is a swimming-pool type research reactor producing neutron fluxes up to 10^{14} neutrons per cm^2 per second when it is operated at a maximum power output of 5 MW (thermal). It utilises enriched uranium ($\sim 93 \%$ U-235) and is moderated and cooled with light water. The open pool concept provides easy access to the reactor core and its experimental facilites, making it a very versatile facility.

The currently available facilities at the McMaster Nuclear Reactor are listed in Table 1 and their locations are shown in Figure 1. The details of these facilities are available in the literature (41) and will therefore not be repeated here. Suffice it to say, the present work was performed at beam port No. 2 employing a 50 mm x 10 mm rectangular beam of fast-epithermal neutrons. The engineering aspects of shaping and shielding of this fast neutron beam will be discussed in subsequent sections.

Table 1

Current MNR Facilities

A. Beam Ports   4 at 152 mm at core (#1, 3, 4, and 6)
2 at 203 mm at core (#2 and 5)

B. Tangential Tubes 1 horizontal
1 vertical

C. Irradiation Positions

    I Capsules   1 In-Core
4 Graphite Reflectors
1 Beryllium Reflector
1 Graphite, Low Flux

    II Rabbits   1 In-Core terminal
2 Fixed terminals.

D. Special Facilities

    I   FLUMP   Flux Mapping Facility

    II   RIFLS   Reactor Irradiation Facility for Large
Samples

    III SAGE   Spent Assembly Gamma Exposure Facility

    IV SNERF   Submersible Neutron Experimental and
Radiography Facility

    V   HOT CELL   Housing 5 kCi Co-60 source

    VI GAMMA ROOM

Figure 1

The MNR Facilities

2 RABBIT TERMINALS

SNERF

FLUMP

B.P.6

B.P.5

REACTOR

CORE

B.P.4

B.P.3

B.P.2

B.P.1

VERTICAL TANGENTIAL TUBE

IN-CORE CAPSULE OR RABBIT IRRADIATION POSITION

BARYTES CONCRETE

HORIZONTAL TANGENTIAL TUBE

LEGEND

GRAPHITE REFLECTOR

BERYLLIUM REFLECTOR
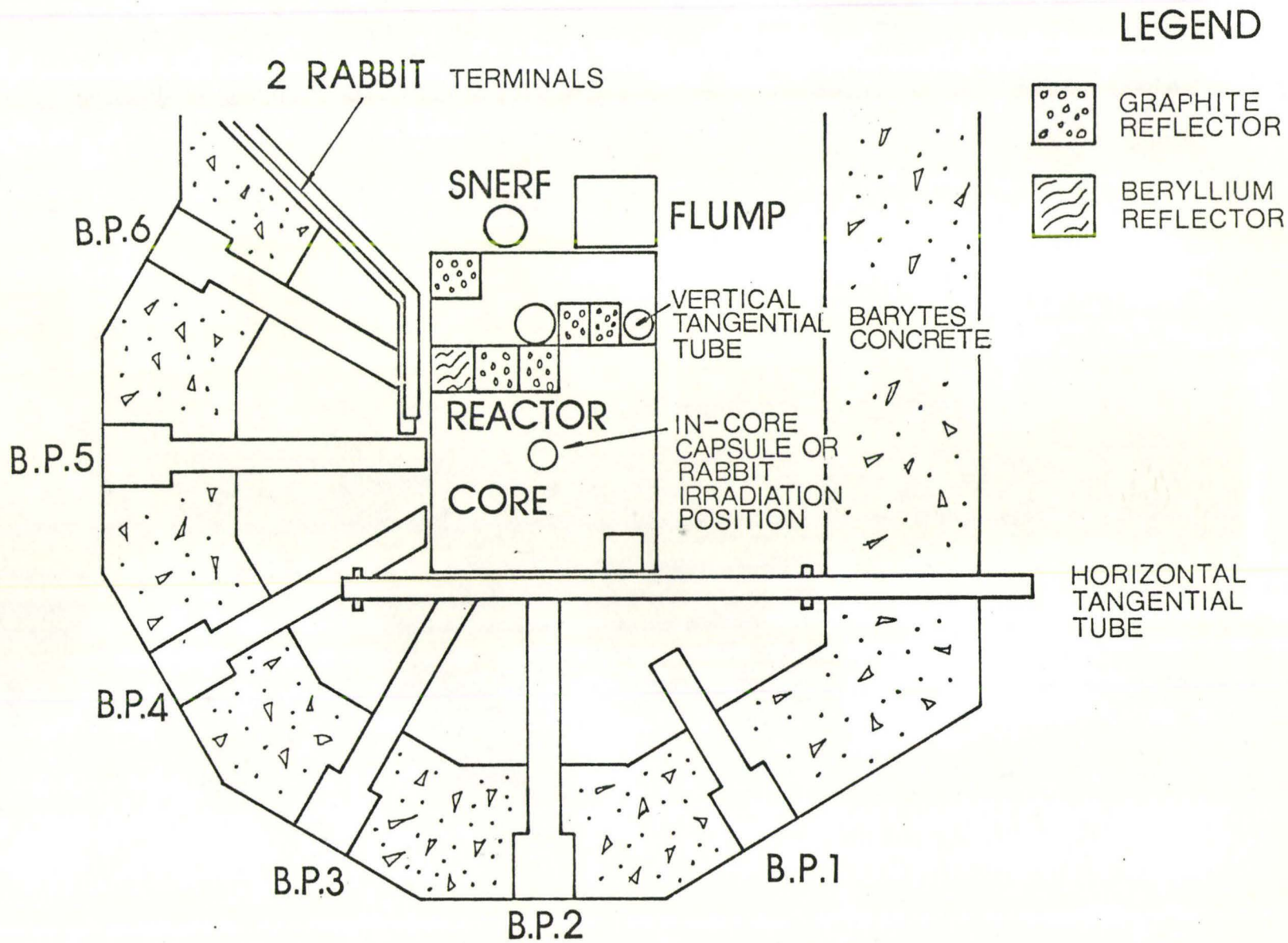
2.2 Collimation of the Neutron Beam

Fission neutrons from the reactor core were collimated by a series of collimators some of which were specially made for the experiment. Figure 2 shows the sectional view of the collimator holder system inside the 1.8 m barytes concrete reactor pool wall at beam port No. 2. Two barytes concrete cylinders C_1 and C_2, each of 213 mm diameter and 381 mm long first collimate the neutrons into a cylindrical beam of 64 mm diameter with its 64 mm centre bore. Four more similar concrete cylinders C_3, C_4, C_5 and C_6 with 114 mm centre-bore, when lined up one after the other inside the beam port secure a cylindrical aluminum collimator holder in position as shown in the figure. This cylindrical collimator holder is separately shown in Figure 3. It consists of an aluminum cylinder with 102 mm ID and 3 mm thick wall and 1.50 m long with a face plate at one end. The aluminum face plate is 13 mm thick and 533 mm in diameter. Eight holes each 14 mm in diameter are drilled through the face plate on the circumference of a circle 483 mm in diameter. Each hole is separated from its neighbour by 45°. The collimator holder can thus be further secured onto the reactor pool wall with bolts through the eight holes on the face plate onto holes tapped through the reactor wall. The cylindrical neutron beam previously collimated by C_1 and C_2 is further collimated by a collimator inserted into the collimator holder.

Figure 2

Secondary Concrete Neutron Collimation System inside the
Beam Tube and Holder for the Primary Beam Collimator

POOL WALL

REACTOR POOL

COLLIMATOR HOLDER

BEAM PORT LINER

C_1 C_2 C_3 C_4 C_5 C_6

1500

102

64
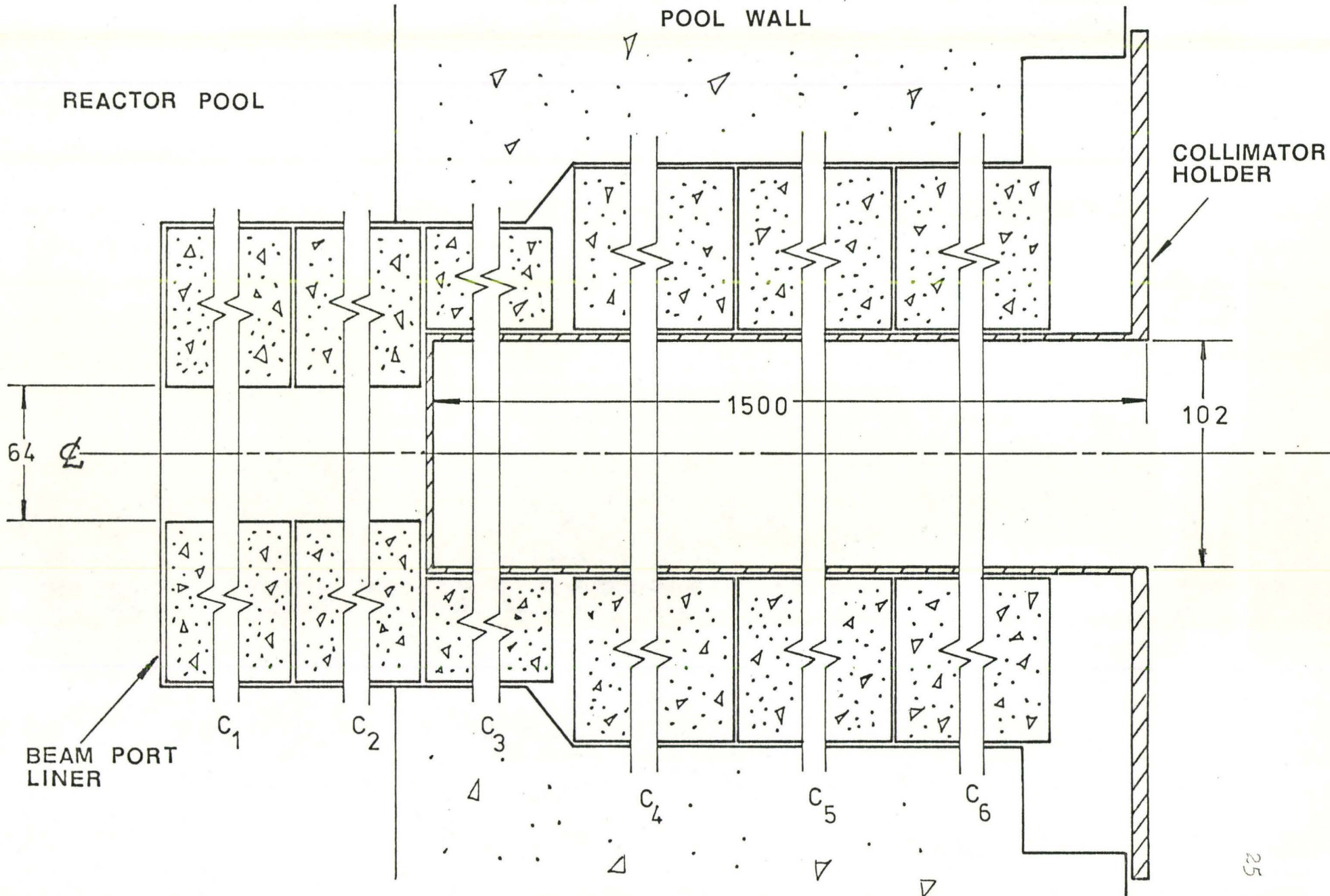
DIMENSIONS ARE IN MILLIMETRES

Figure 3

Aluminum Holder for Primary Beam Collimator

533 Dia

1500

102

483

Ø13.4
8 HOLES EQ SP

102

DIMENSIONS ARE IN MILLIMETRES

27
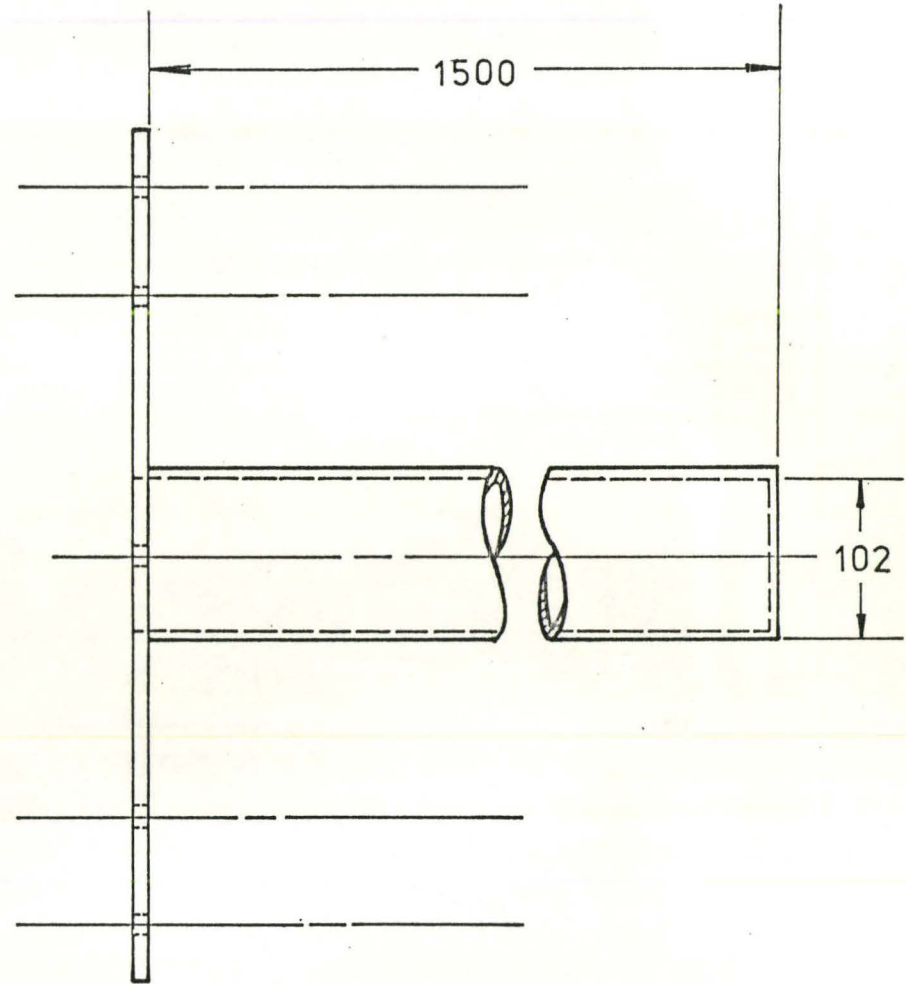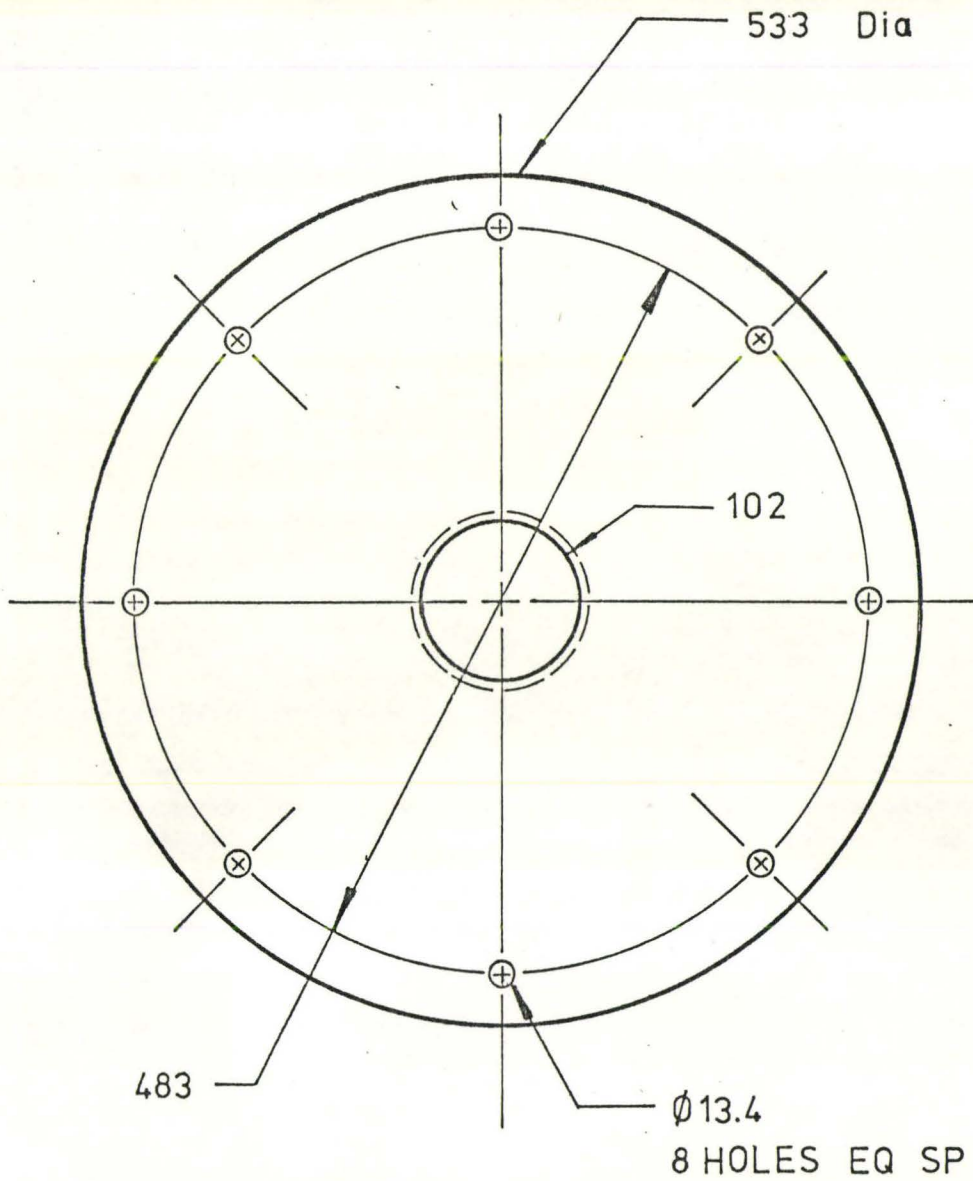
The collimator is an assembly consisting of two identical sections. Each section consists of an aluminum cylindrical housing enclosing a rectangular perspex 'tunnel'. Figure 4 shows both the front and side views of the perspex tunnel. Notice that although the interior cross-section of the perspex tunnel is uniform throughout the whole length, the wall thickness is greater for half the length of this tunnel, resulting in a 'step' in the wall thickness. Near each end of the tunnel, there is a set of four threaded holes each accommodating a positioning screw. After inserting the perspex tunnel into the cylindrical housing, by adjusting the positioning screws, the axis of the perspex tunnel could be aligned with that of the cylindrical aluminum housing.

Figure 5 shows the aluminum housing with the perspex tunnel properly aligned and held in position. One end of the cylindrical housing was closed with a circular end plate. A small amount of melted paraffin wax was poured in the space between the perspex tunnel and the housing. An equal amount of borax powder was added to the wax. The mixture was well mixed and left aside to cool and solidify. After the first layer of the mixture of wax and borax had solidified this process was repeated to obtain a second layer and so on until all the space between the perspex tunnel and the housing wall was filled. This time-consuming operation was necessary as the borax powder does not dissolve in melted wax and tends to sink. In this way, a relatively more uniform mixture of

Figure 4

Perspex 'Tunnel' in Primary Beam Collimator

DIMENSIONS ARE IN MILLIMETRES

30

wax and borax powder can be obtained.

As a final step, the remaining end of the cylindrical housing is closed with an end plate with a pair of connectors welded on. Figure 5 shows the front and side views of two such end plates, one for each collimator housing. The connectors on one end-plate are male (hooks) while those on the other one are female (eyes). In mounting the collimator, the collimator with the female connector is first slipped into the collimator holder positioned on the reactor pool wall with the 'eyes' facing away from the pool. The other section is then inserted into the collimator holder with the hooks facing the pool. By rotating the outer collimator clockwise, the outer collimator section can be engaged onto the inner one and the whole collimator system can be rotated. Turning the outer collimator in the anti-clockwise direction will disengage the two collimators.

Fast neutrons, on collisions with the hydrogen in the paraffin wax lose energy and slow down. The boron in the borax powder is a 1/v absorber and absorbs the slowed neutrons. Hence, the combination of wax and borax can absorb fast neutrons. The perspex, being rich in hydrogen, also removes neutrons. Thus, neutrons can only go through the rectangular 'tunnel' in the middle of the perspex tunnel and hence are collimated.

The step in the perspex 'tunnel' is designed to prevent streaming of neutrons through any possible space

Figure 5

Primary Beam Collimator (One Section)

POSITIONING
SCREW

PERSPEX
TUNNEL

TUNNEL
HOUSING

END
PLATE

HOOK

EYE
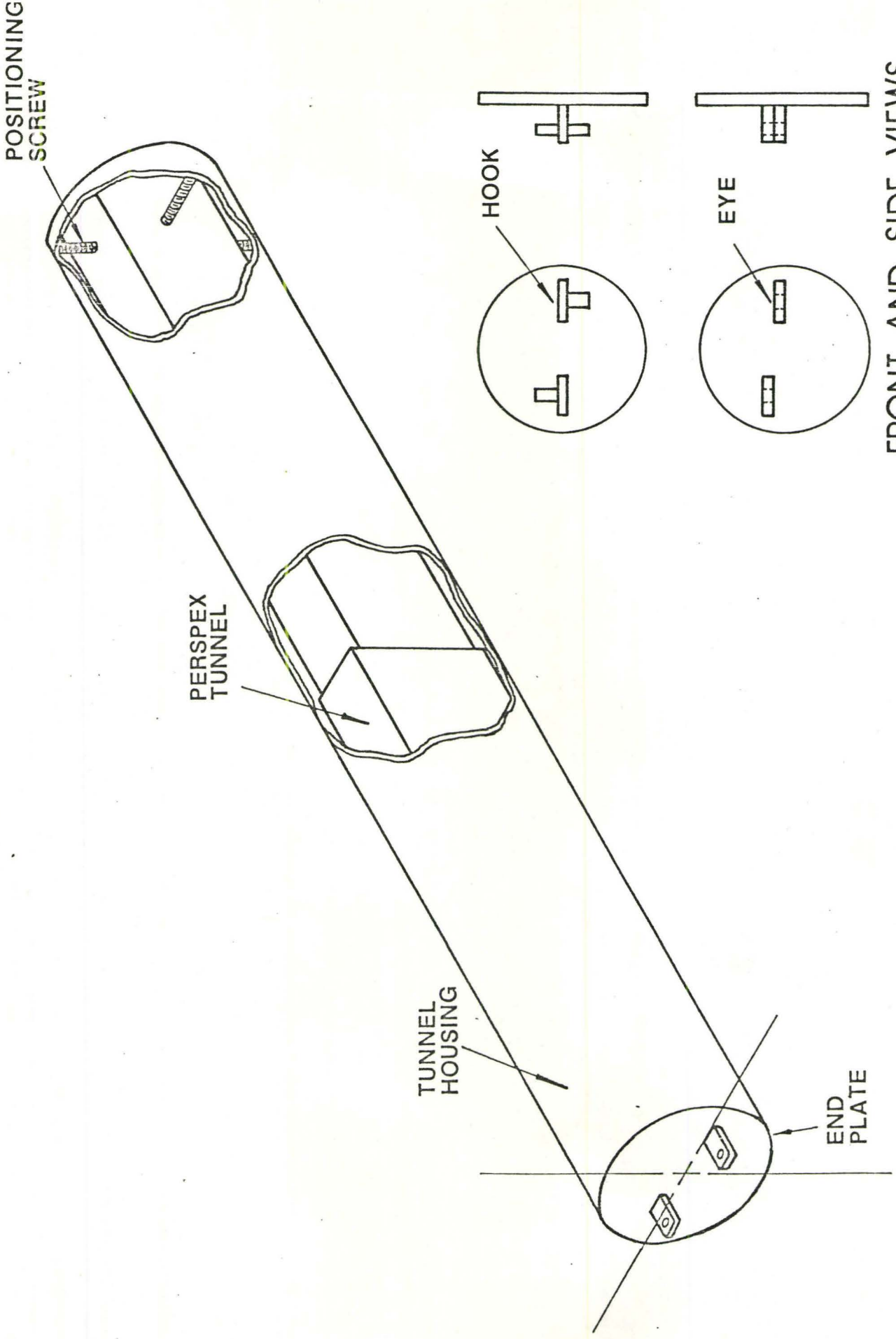
FRONT AND SIDE VIEWS
OF END PLATES

between the solidified wax and the wall of the perspex tunnel.
Any streaming through cracks in one section will be stopped
by the wax or perspex in the other section.

After collimation, the neutron beam is available for
the experiment. However, in order that the experimenter can
open or close the beam at will, a beam shutter system is
necessary. This shutter system will be discussed in the next
section.

2.3 Beam-Shutter System (Tank)

The Beam Shutter System consists of a beam shutter
tank, a beam shutter pipe, and water draining system. The
beam shutter tank is a 0.914 m x 0.914 m x 0.914 m aluminum
cubical tank with a wall thickness of 3 mm. It is supported
by four legs 380 mm from the ground. Figure 6 shows the front
and side view of the shutter tank. Two holes, one of 127 mm
diameter and one of 203 mm were drilled through the centres
of the front and rear faces respectively to accommodate a
stepped shutter pipe as shown in the figure. The length of
shutter pipe is 1.07 m.

For the first 610 mm the circular cross-section of
the shutter pipe is 127 mm in diameter. The diameter is
increased to 203 mm after 609 mm, providing a step S as shown
on the side view in the figure. At the rear end (203 mm
diameter), the shutter pipe is closed with an end-plate 25 mm
from the rear end of the pipe. This shutter pipe is welded
onto the two holes drilled on the front and rear faces.

Figure 6

Beam Shutter System

914

457

203 Dia

914

127 Dia

914

25

457

368

P

S

152

457

457

DIMENSIONS ARE IN MILLIMETRES

36
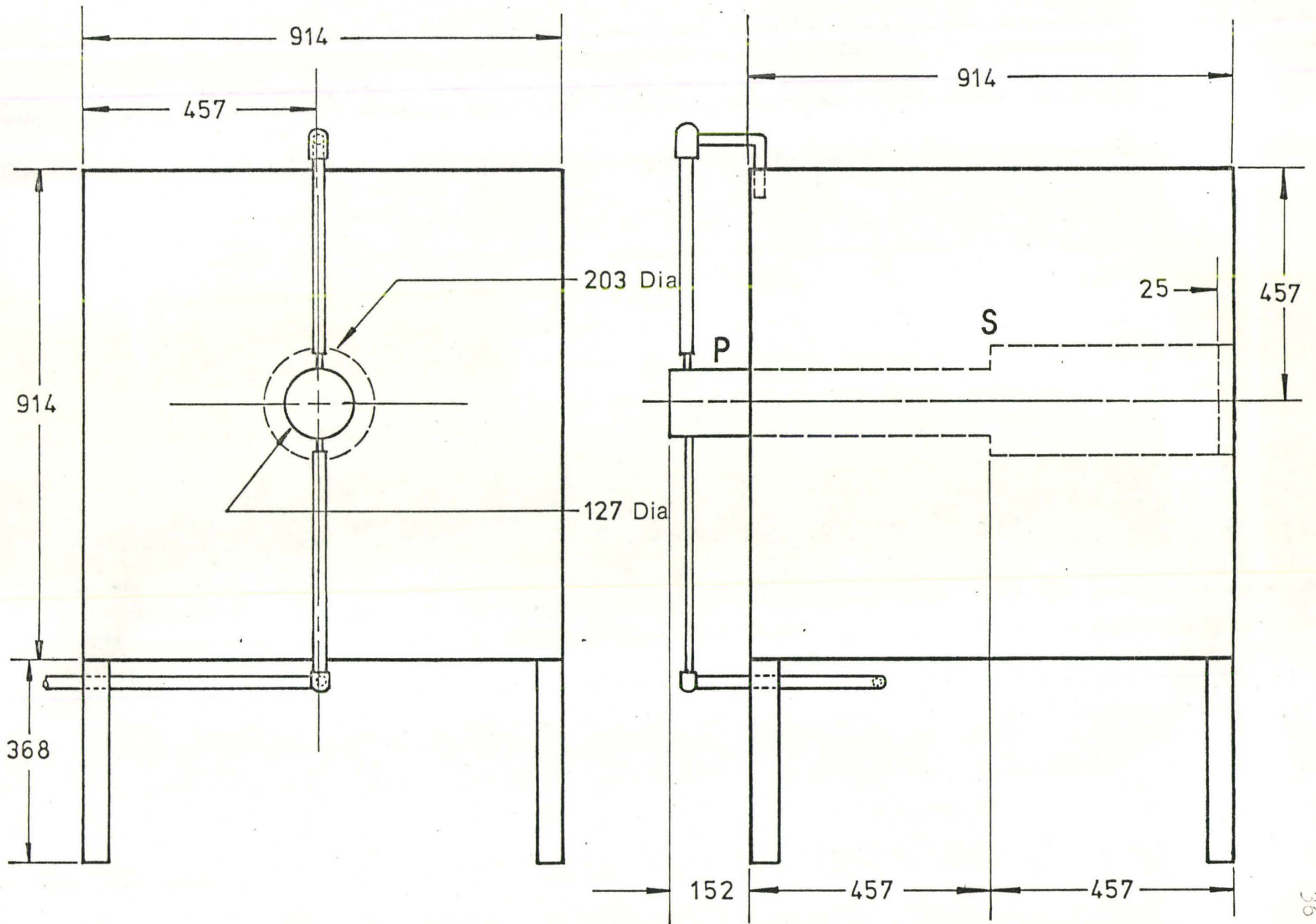
Since the total length of shutter-pipe exceeded that of the shutter tank, a portion of 152 mm of the shutter pipe protrudes on the outside of the tank. For ease of description, this portion of the shutter pipe will be designated P. The bottom of the portion P of the shutter pipe is attached to a plastic water bag of 19 litres capacity with copper piping and tygon hose. The shutter pipe can thus be filled or emptied by raising the water bag above, or lowering it below, the level of the shutter pipe. The top of the portion P of the shutter pipe is opened to a bent copper pipe venting back into the shutter tank. Hence, water can overflow into the shutter tank from the shutter pipe if necessary during filling.

During a reactor shut-down, the shutter tank system was moved against the reactor pool wall and the axis of the shutter pipe was aligned with that of the collimator. Both the shutter tank and shutter pipe are filled with water. When the reactor is started up, the collimated neutron beam is stopped by the water in both the shutter pipe and shutter tank. The sudden change in the diameter of the shutter pipe at S will prevent streaming of neutrons along the aluminum wall of the shutter pipe. All straight-line paths for streaming are eliminated by the design of such a 'step' in the shutter pipe. To open the beam port, one drains the shutter pipe by emptying the water in it into the lowered water bag.

When the beam is turned on, neutrons will enter the experimental area, increasing the background statistics for

experiments run in other beam ports as well as causing poten-
tial health hazards to by-standers (the safety limit for
visitors being 2.5 mR/hr). For these reasons, a shielding
system to contain these neutrons was necessary.

2.4 Shielding System

The shielding system is composed of two shielding
water tank, two beam catchers, and two wax boxes. Figure 7
shows the top view of the shielding system surrounding an
experimental 'cavity' on the beam port floor. The beam shutter
system is flanked by two shielding water tanks S1 and S2.

The two shielding water tanks S1 and S2 are rectangular
tanks 2.997 m x 1.625 m x 0.381 m and made of carbon steel.
When filled with water, they provide effective shielding
against scattered neutrons with the beam turned on. The gaps
between the two shielding tanks and the shutter tank are
each shielded by a wooden box WB1 or WB2 0.305 m x 1.448 m
x 0.305 m filled with solid paraffin wax blocks.

Transmitted neutrons are collected by two beam catchers
BC1 and BC2. Beam catcher BC2 is a carbon steel water tank
with the dimensions shown in Figure 7. Beam catcher BC1 is
a rectangular tank 0.813 m x 1.397 m x 0.610 m as shown in
Figure 8. Two ports of 229 mm diameter were cut into the
front and rear faces and a cylindrical pipe of 229 mm diameter
was welded into these two ports forming a 'tunnel'. The
centre of the pipe is 0.826 m above ground, i.e. at the same
level as the neutron beam. The rest of the space in the tank

Figure 7

Shielding System against Neutrons and Gamma Rays around Beam

Port No. 2

SS   SHUTTER SYSTEM

S1, S2 2.997 m x 1.625 m x 0.381 m SHIELDING WATER TANK

BC1   LEADED BEAM CATCHER

BC2   WATER BEAM CATCHER

WB1, WB2 WAX BOX

REACTOR POOL WALL

S1

WB1

SS

WB2

S2

BC1

BC2

0.406

1.270

0.813

0.406

0.305

0.305

1.981

0.610

0.20

0.508
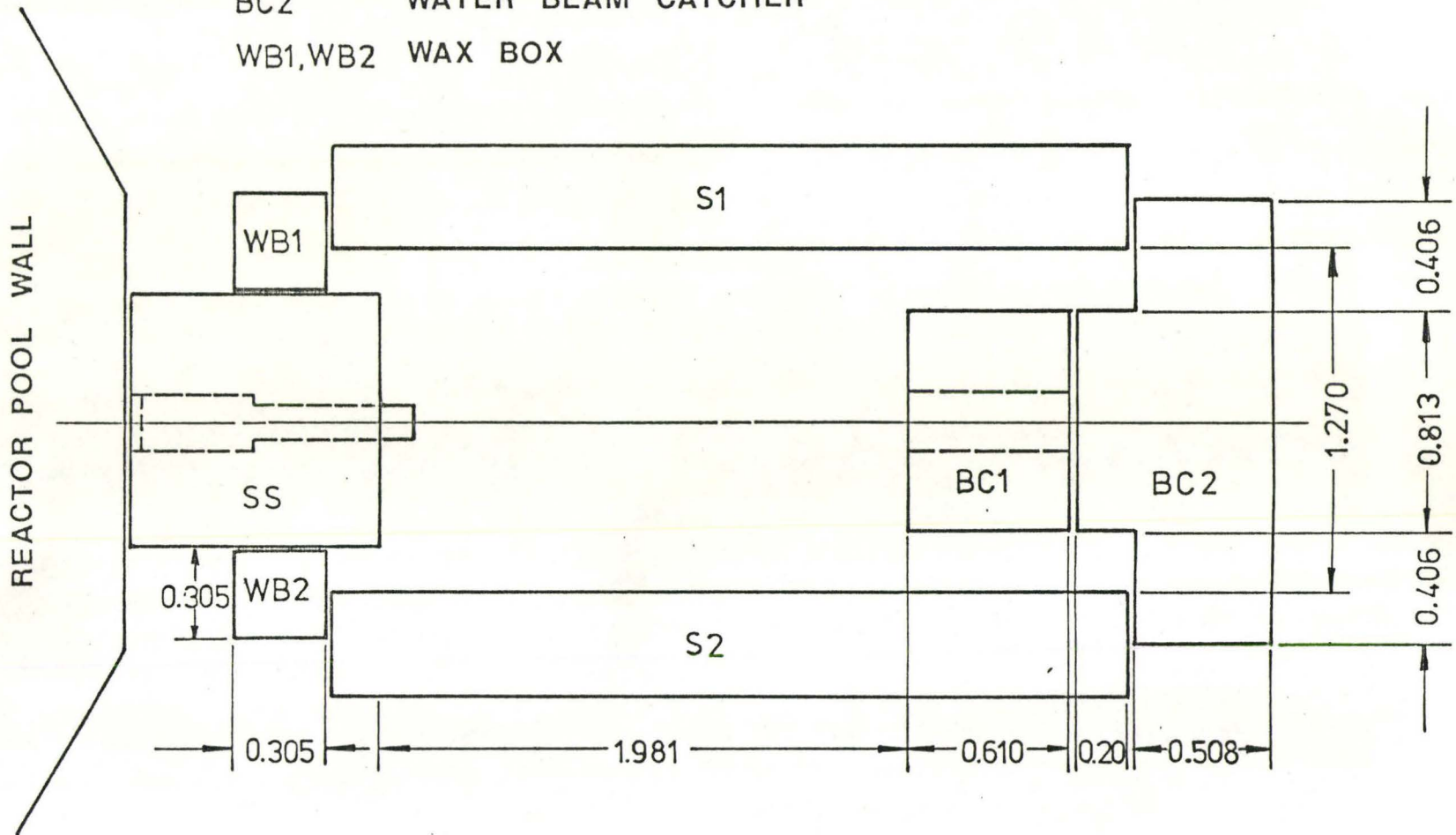
DIMENSIONS ARE IN METRES

Figure 8

Beam Catcher BC1

826

610

229 Dia

813

1397
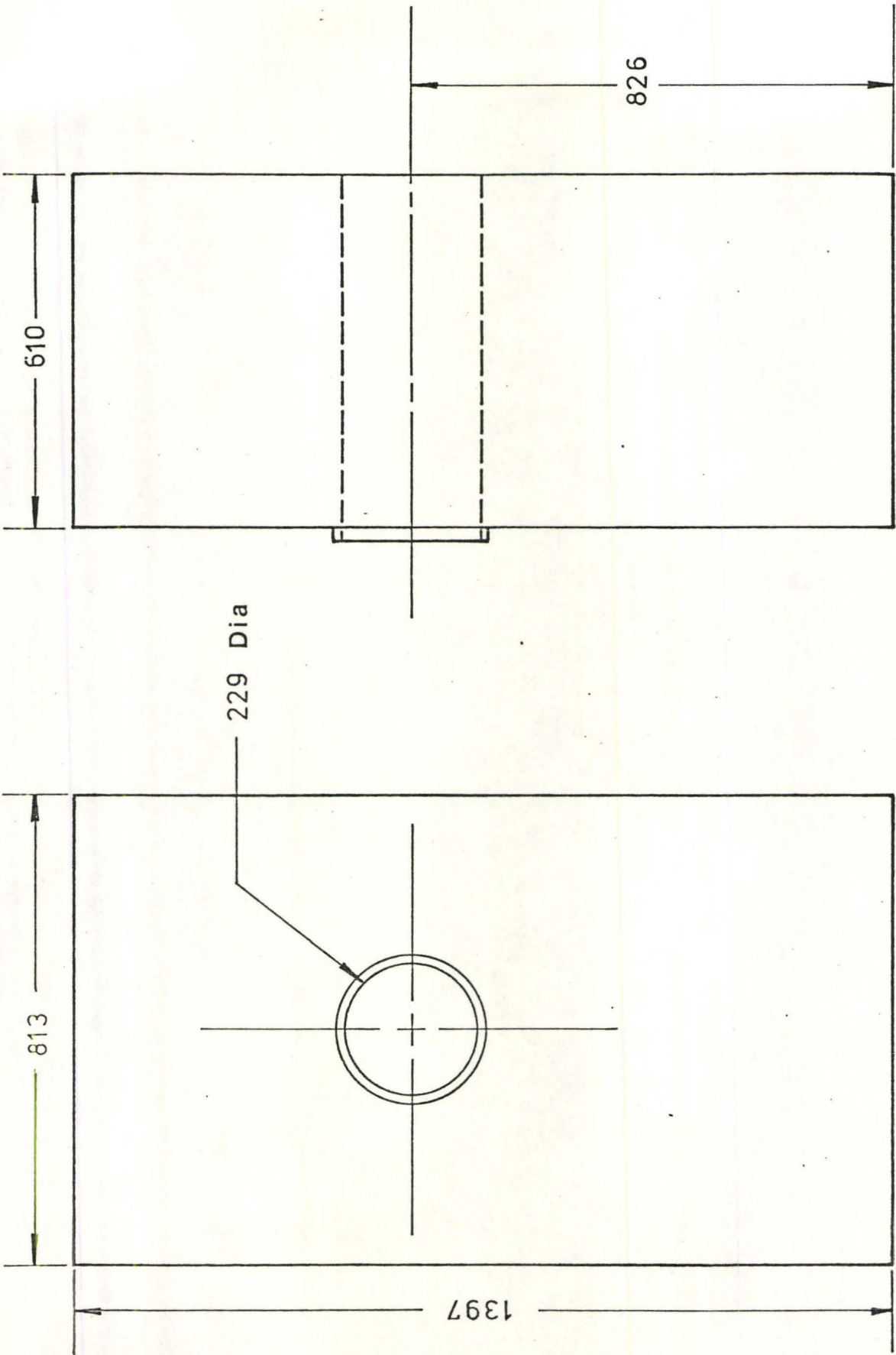
DIMENSIONS ARE IN MILLIMETRES

is filled with solid paraffin wax.

The transmitted beam passes through the cylindrical 'tunnel' in beam catcher BC1 and is stopped by the water in beam catcher BC2. Neutron back scattered by BC2 will be attenuated by the paraffin wax in beam catcher BC1. Although the neutron flux seen by BC1 and BC2 is much higher than S1 and S2 (BC1 and BC2 being directly in the beam), the two beam catchers together provide sufficient shielding in the beam path area.

Gamma rays that are in the beam are shielded by lead bricks piled up against BC2 outside the experimental cavity. The shielding system together with the shutter tank system surrounds a space available for the test section and experimental equipment.

3 EQUIPMENT AND APPARATUS

Apart from the availability of a collimated fast neutron beam and the shielding system, the experiment in the present work also requires the set-up of a test section (target), neutron detectors, and associated electronics.

3.1 Test-Sections

In the present work, two test-sections were built. In one test-section, the vapour phase is simulated by aluminum since this metal is quite neutron transparent (aluminum-water test section). In the other, air and water are well mixed in the test section by passing air and water vertically

down a flow loop (air-water test section)

3.1.1 Aluminum-Water Test Section

A test section assembly made of aluminum was built to house both the aluminum-water test section and neutron detectors. Figure 9 shows the key components of the test section assembly. The base plate A is mounted on a rec-tangular dexion frame 0.406 m long, 0.305 m wide, and 0.737 m high. At each bottom corner, the dexion frame is welded to an adjustment bolt so that the elevation of the frame can be adjusted to within 25 mm.

The spacer B has a circular slot whose centre coin-cides with that of the semi-circular portion of the base plate. The specimen holder D, when inserted into the circular slot in B provides a turning pivot for the rotating arm C on which the neutron detector sleeve holder E rests. The specimen holder D, apart from providing a turning pivot for the rotating arm C, houses different aluminum target specimens simulating different void fractions when the rest of the space between the inserted specimen and the specimen holder wall is filled with water. Specimen holder of ID's 50.8 mm and 25.4 mm to house 50.8 mm and 25.4 mm specimens respectively are available.

Three flow regimes were simulated by the aluminum specimens, namely, annular flow, inverted annular flow, and stratified flow. In the set of 50.8 mm specimens, for each simulated flow regime, five void fractions were chosen, 0.25,

Figure 9

Test Section and Detector Holder Assembly

A Base Plate
B Spacer
C Rotating Arm
D Specimen Holder
E Detector Sleeve
   Holder
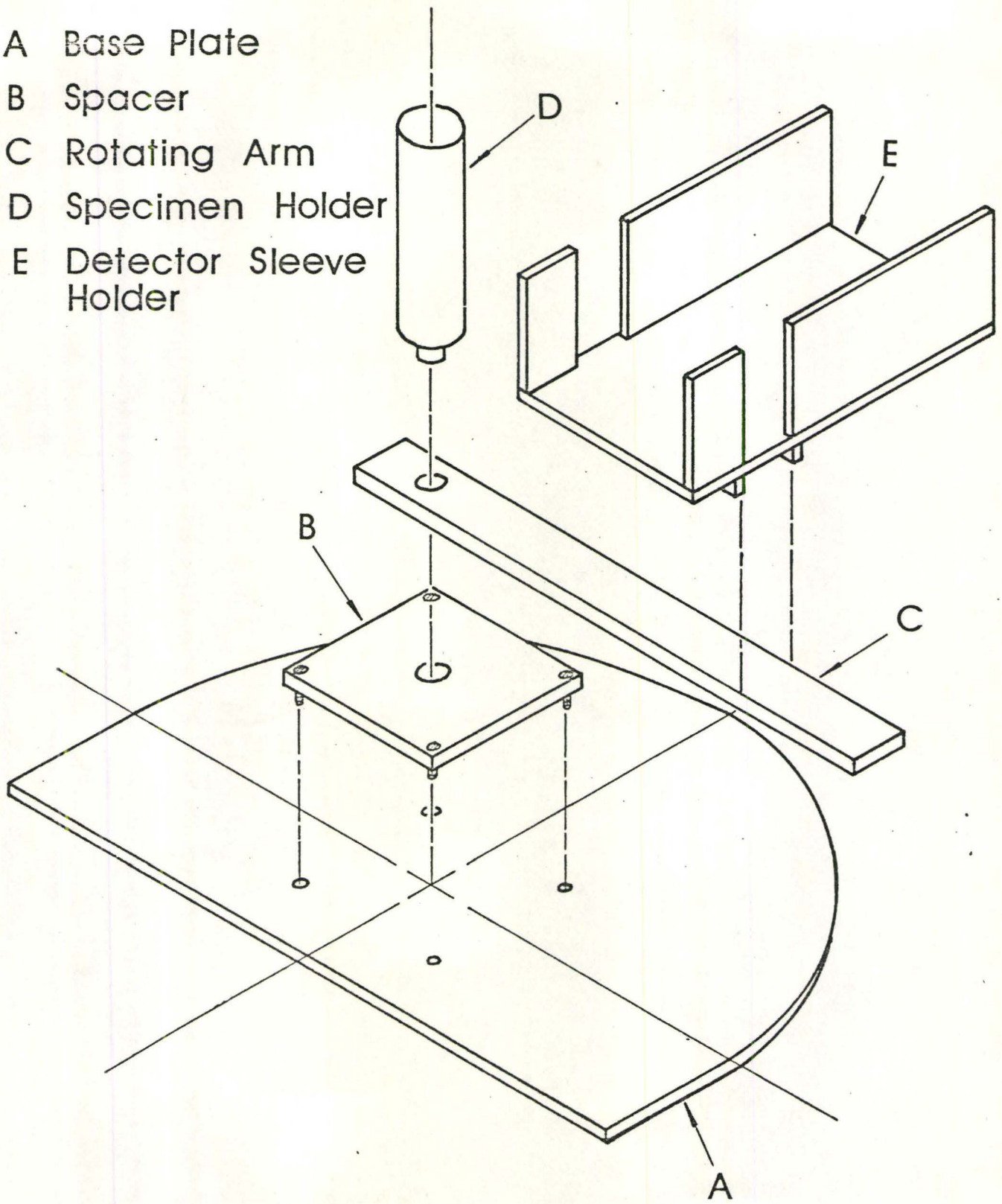
0.50, 0.65, 0.75, and 0.90. In the set of 25.4 mm specimens, void fraction of 0.25, 0.50, and 0.75 were available. These specimens and their dimensions are shown in Figure 10 and Table 2.

The neutron detector used in this experiment (see section 3.2) is shielded against background neutrons by a detector sleeve. The neutron detector sleeve consists of two parts P1 and P2 as shown in Figure 11. Each of P1 and P2 consists basically of two aluminum cylinders, one inside the other, held in position by two end plates. Both the end plates in P1 have a hole in the centre so that a cylindrical neutron detector can be inserted into the inner cylinder. The part P2 is shorter and has one end closed. The space between the inner and outer cylinder in both P1 and P2 is filled with borax powder which absorbs thermal/epithermal neutrons efficiently. The two parts P1 and P2 are placed between the vertical plates of the neutron detector sleeve holder with their axes perpendicular to the rotating arm and flush against either end of the neutron detector sleeve holder. Since P1 and P2 are separated by 50 mm, a neutron detector, when inserted into the inner cylinder of P1 and P2 will have an effective detection width of about 50 mm.

3.1.2 Air-Water Test Section

In order to further check the feasibility of this void measurement technique using neutron scattering, an air-water flow loop was built so that experiments could be done in a flowing two-phase system. Figure 12 is a schematic

Figure 10

Specimens simulating Voids in Aluminum-Water Test Sections

49
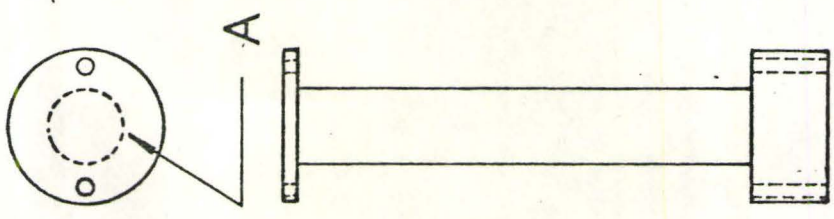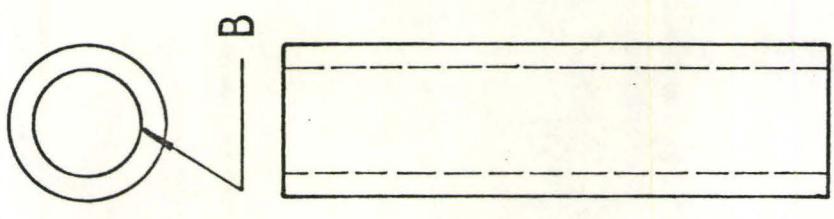
STRATIFIED
FLOW
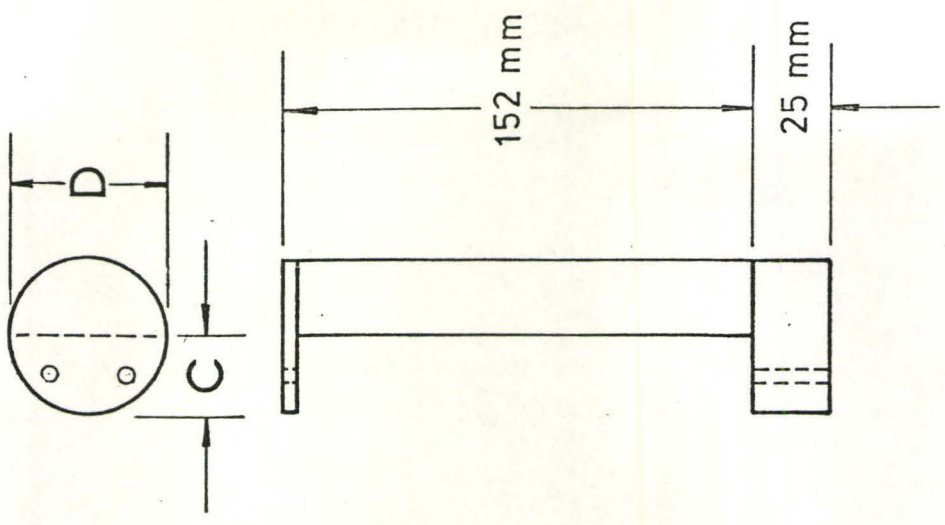
INVERTED ANNULAR
FLOW

ANNULAR
FLOW

Table 2

DIMENSIONS OF TEST SECTION SPECIMENS (mm)

(a) 50.8 mm Specimens

Void Fraction	Annular A	Inverted Annular B	Stratified C	D
0.25	25.4	44.0	15.0	46.4
0.50	35.9	35.9	25.4	50.8
0.65	41.0	30.1	31.6	49.3
0.75	44.0	25.4	35.8	46.4
0.90	48.2	16.1	42.9	36.8

(b) 25.4 mm Specimens

Void Fraction	Annular A	Inverted Annular B	Stratified C	D
0.25	12.7	22.0	7.5	23.2
0.50	18.0	18.0	12.7	25.4
0.75	22.0	12.7	17.9	23.2

Figure 11

Neutron Detector Sleeve

305

76

DIMENSIONS ARE IN MILLIMETRES

31 Dia

165

A

A

P1

31 Dia

165

B

B

P2
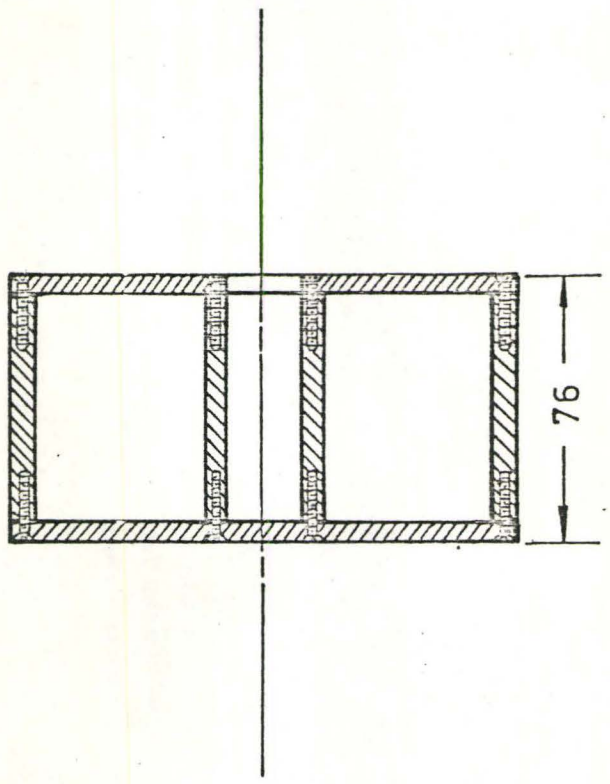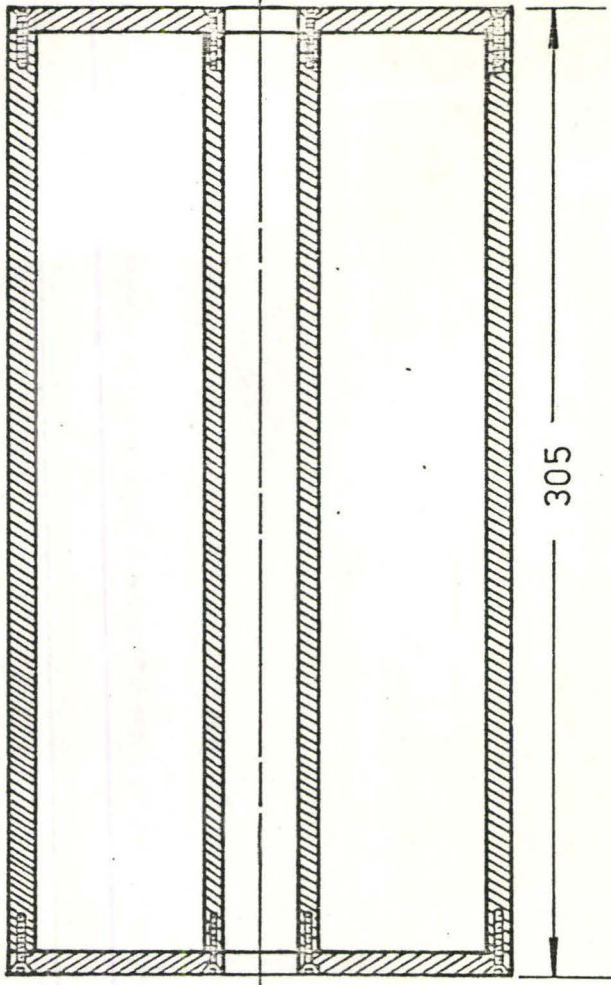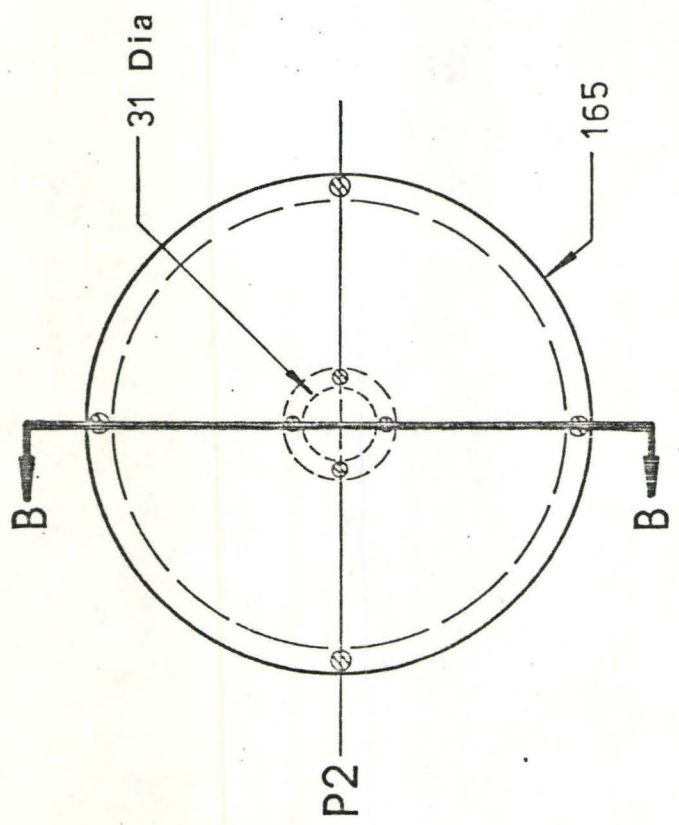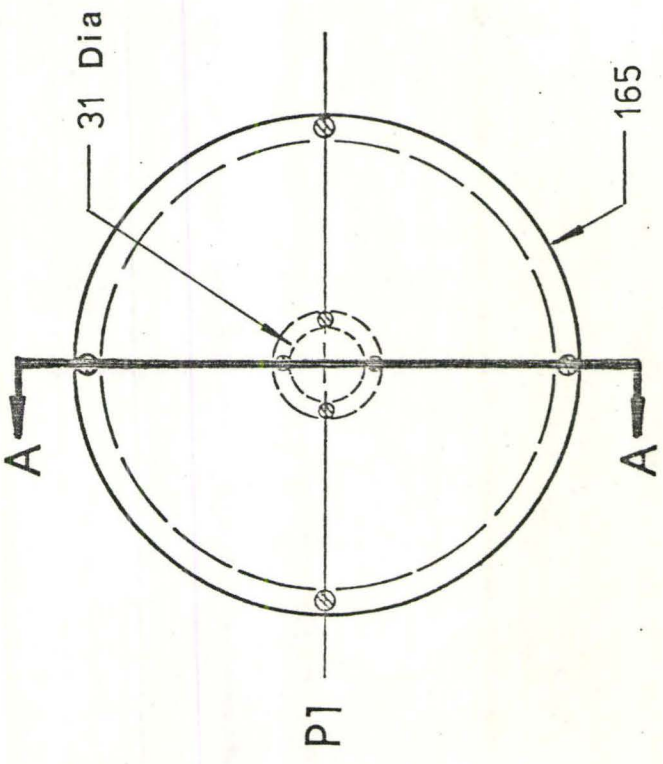
Figure 12

Schematic Diagram of Air-Water Flow Loop

MIXER

INLET SECTION

V_1

ΔP

neutron beam line

TEST SECTION

V_2

EXIT SECTION

V_3

F/M

AIR

F/M

FILTER

V_4

P P

AIR / WATER
SEPARATOR

PUMP
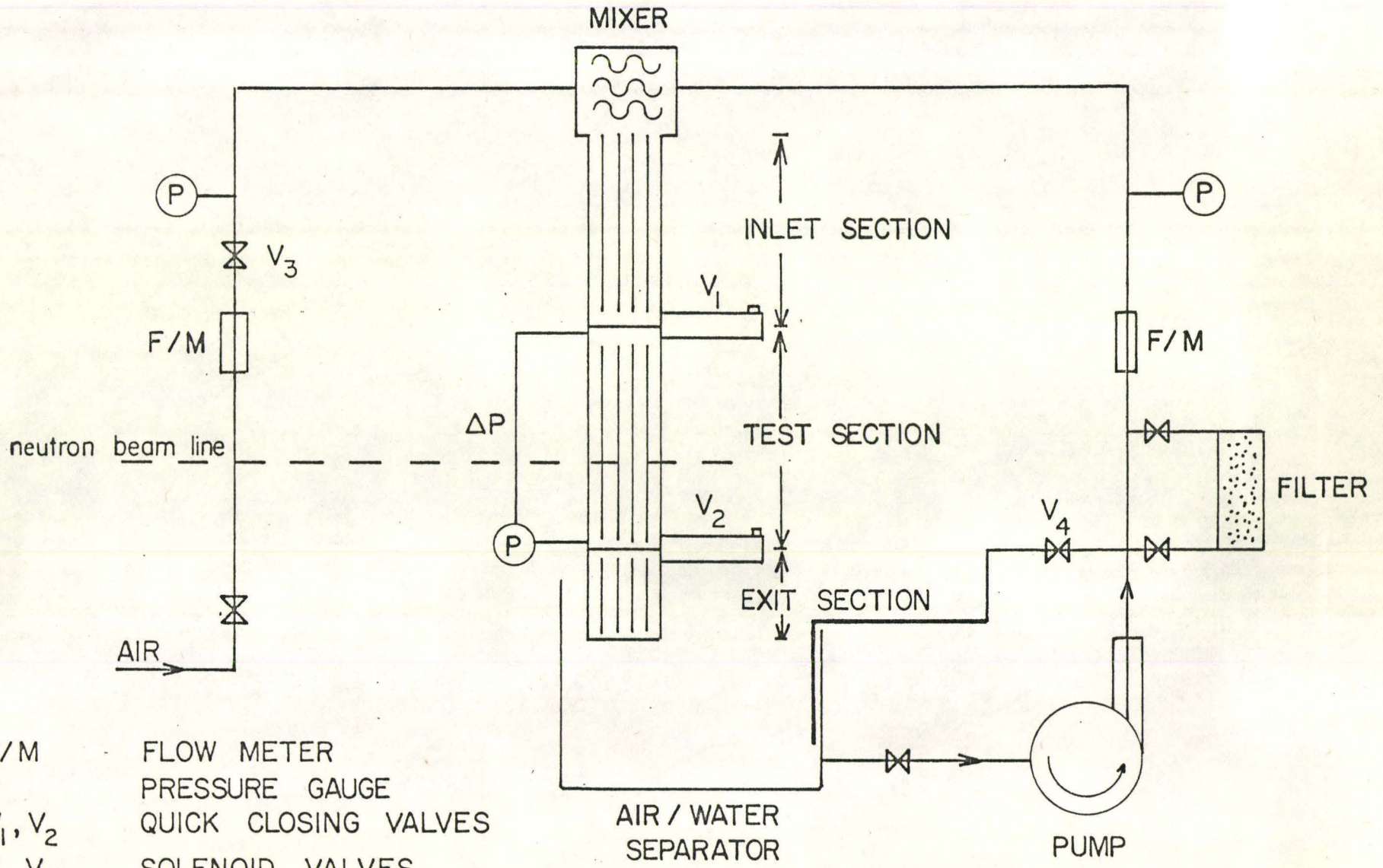
F/M — FLOW METER
P — PRESSURE GAUGE
V_1, V_2 — QUICK CLOSING VALVES
V_3, V_4 — SOLENOID VALVES

diagram of the air-water loop. The test section was an aluminum pipe of 38.1 mm ID and 3.2 mm wall thickness. The inlet and exit sides of the test section could be closed by two quick acting valves V_1 and V_2 separated from each other by 0.587 m. Each valve could be closed in 100 ms. The inlet section was a lucite pipe of the same ID as the test section and was 0.762 m in length. The transparency of the inlet section made visualization of flow patterns possible. The exit section consisted of an aluminum pipe 0.305 m in length and of the same ID as the test section. Both the inlet and outlet sections were required to help develop a quasi-steady air-water flow.

A centrifugal water pump with maximum capacity of 4.42 litres/s pumped water into the mixer made of steel wool situated above the inlet section. In the mixer, the water was mixed with air at pressure up to 6 bars. The air-water mixture, after passing through the test section, emptied into the air/water separator which consisted of a cubic plastic tank 0.457 m on each side and a plastic partition 0.305 m in height, that divided the air-water separator into an inlet and outlet compartment. The air-water mixture from the test section first emptied into the inlet compartment of the air-water separator. Since the water in the inlet compartment could access the outlet compartment of the air-water separator only by overflowing over the partition, the air escaped back into the atmosphere before reaching the pump.

The solenoid valve V_4 remained closed while the two

quick closing valves V_1 and V_2 were open and the pump was on. When V_1 and V_2 were closed, the solenoid valve V_3 and the pump were turned off automatically and V_4 would open, by-passing water from the pump into the air-water separator, and thus releasing residual pressure in the loop. This prevented damage to the quick closing valves V_1 and V_2.

The loop was mounted on a dexion frame with the test section held in a vertical position. The neutron beam was made incident on the test section as shown in the figure. A neutron detector was placed at the same level as the beam and at 90° to both the beam and the test section. The detector sleeve (see section 3.1.1) was adjusted so that the effective detection width of the detector was 38.1 mm (same dimension as the test section) to count the scattered neutron flux.

3.2 Neutron Detectors

The detection of neutrons requires some type of interaction between neutrons and the detector. There are several mechanisms by which the interaction with matter takes place and each of these is the basis of a potential method of detection. The most useful ones are as follows (42):

(a) neutron-induced transmutations in which the product particles make detection possible. Examples are (n, α), (n,p), (n, γ), and (n, fission) reactions.

(b) neutron-induced transmutations which result in radioactive nuclei giving information on the neutron flux that induced the radioactivity.

(c) elastic scattering of neutrons in which the recoil

particle is charged and is capable of being detected.

In the present work, two kinds of neutron detectors employing process (a) have been used. They are He^3 and BF_3 neutron detectors.

3.2.1 He^3 Detectors

The availability of He^3 made possible an important method of neutron detection, the reaction being (43)

$$He^3 + n \longrightarrow H^3 + p + 765 \text{ keV}$$

where 765 keV is the Q value of the reaction and is the difference between the sum of rest masses for the system of particles before and after the reaction.

This reaction has good properties for neutron detection. The cross section, starting with 5400 barns for thermal neutrons, varies smoothly over the entire energy range of interedt, having no resonances. There are no excited daughter products, and so the reaction products, the triton and proton, contain the entire energy in each reaction.

From a simplified view point, a He^3 neutron detector consists of He^3 gas contained under pressure with a mixture of Kr and CO_2 in a cylindrical metal tube. A thin wire suspended at the centre of the tube is positively biased at about 1 to 2 kV while the metal case is grounded. These serve as an anode and a cathode. The triton and proton, being charged (positive) particles, will dissipate all their shared energy in the reaction by ionizing atoms around them producing ion-pairs. The number of ion-pairs is proportional

to the total energy of the triton-proton system, which is in turn linearly related to the kinetic energy of the incident neutron. These ion-pairs are collected at appropriate electrodes giving rise to a pulse whose size then varies linearly with the kinetic energy of the incident neutron. The signal is then sent through a charge-sensitive preamplifier (see section 3.3.1)

3.2.2 $\underline{BF_3 \ Detectors}$

The configuration of a Boron-Trifluoride-Filled gaseous Detector is similar to that of the He^3 detector discussed in section 3.2.1. The boron isotope employed is B^{10}. The reaction employed in the detection of neutrons is

$$B^{10} + n^1 \longrightarrow Li^7 + \alpha^4 + Q$$
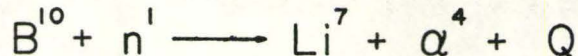
where Q is the reaction energy and attain the value of 2.30 or 2.78 MeV. The latter value corresponds to a direct population of the ground-state of Li^7. The former value corresponds to the population of an excited state of Li^7 with excitation energy of 0.48 MeV leading to a subsequent emission of a 0.48 MeV gamma photon on de-excitation.

The detection process of neutrons with a BF_3 detector is similar to that mentioned in section 3.2.1. The only difference is that the formation of ion-pairs is effected by Li^7 and the α-particle. The cross-section of $B^{10}(n, \alpha)$ reaction has a $1/v$ dependence up to 30 keV.

3.2.3 Comparison between He^3 and BF$_3$ counters

The He^3 detector is more efficient than the BF$_3$ detector in the detection of thermal neutrons (a reaction cross-section of 5400 barns for He^3 compared with 3840 barns for B^{10}). The cross-section varies smoothly for He^3 while there are resonances in the neutron cross-section for B^{10}. Also, He^3 does not disassociate in the presence of gamma rays as does BF$_3$. Therefore, it is suitable for application in a high gamma field.

3.3 Associated Electronics

The output signals from the detector are too small in magnitude for counting instruments. Also, very often one may wish to count only pulses corresponding to neutrons of energy within a certain range (gating). Thus, associated electronics are necessary to amplify the detector output signals and/or to select pulses for counting. Most of these electronic equipment are available commercially as 'plug-in' standard Nuclear-Instrument-Modules (NIM). Details of the circuitry of these Nim modules can be found in the literature (45) and will not be repeated here. However, the function, particularly the characteristic input-output, of the electronics used will be discussed.

3.3.1 Charge-Sensitive Preamplifier

Charge-sensitive preamplifiers are typically of two types (a) ac-coupled and (b) dc-coupled. In either case, the preamplifier is suited for measuring the kinetic energy of the detected neutron, because it integrates the charge on

a feedback capacitor. Thus, the detection of a neutron results in a fast rise and slow decay voltage pulse at the preamplifier output (see Figure 13). The voltage output V_O and decay time τ_t are respectively given by

$$V = Q_D / C_f \tag{13}$$

$$\tau = R_f C_f \tag{14}$$

where Q_D = charge released by the detector

C_f = feedback capacitor

R_f = feedback resistance

The charge-sensitive preamplifiers used in the present work are HARSHAW NB-28 General Purpose Preamplifiers.

3.3.2 Linear Amplifier

A Linear Amplifier takes a preamplifier output at its input. Through CR-RC pulse shaping, the linear amplifier output is semi-Gaussian shaped (unipolar) and the height of the centroid is proportional to that of the preamplifier output signal. Alternatively, through double differentiation, with CR-RC-CR pulse shaping, the linear amplifier output extends both above and below the baseline (bipolar) with the centroids being proportional to the preamp output (see Figure 13).

The linear amplifiers used in the present work are HARSHAW NA-23 Amplifiers.

3.3.3 Delay Amplifier

A delay amplifier inputs an analog signal and

reproduces it at its output (unit gain) at a later preset
time interval (micro-second range). It is useful in setting
SCA windows (see section 4.1) An ORTEC 427 delay amplifier
is used in the present work.

3.3.4 Single Channel Analyser (SCA)

A Single Channel Analyser (SCA) marks the occurrences
of linear amplifier output pulses that meet certain restric-
tions placed on their amplitudes (pulse heights). This instr-
ment has both a lower-level and upper-level discriminator
that can be set to define a certain amplifier output. The
region between the lower-level and upper-level discriminator
settings is called the SCA window. Pulses whose amplitudes
fall within the window are marked by a logic output from the
SCA. This logic output can be counted by a scaler or used
to trigger other NIM modules such as a linear gate. Single
channel analysers used in the present work are HARSHAW NC-12
SCA's.

3.3.5 Linear Gate

A Linear Gate has two inputs, one for linear input
and one for gate input. The linear input normally accepts
analog (linear amplifier output) pulses. The Gate input
takes logic pulses from an SCA. When the linear gate
encounters gating input from the SCA, the 'gate' inside is
opened for a fixed time interval ($\sim 20\mu$s). If an analog
pulse happens to enter the linear gate during this time
interval this analog pulse will be let through the gate and

appears at the gated output. Pulses that arrive at times when the gate remains closed will be grounded. This instrument is useful in coincidence counting and setting windows for the SCA. The linear gate used in the present work is an ORTEC 426 Linear Gate.

3.3.6 Multichannel Analyser (MCA)

A Multi-Channel-Analyser (MCA) essentially consists of an Analog to Digital Converter (ADC) and a memory bank (channels). When an analog pulse of a particular height V enters the ADC, it is analysed according to its height by the ADC. One count is then added to a channel in the memory which is linear with respect to pulse height and stores the number of counts corresponding to heights $V \pm \Delta V$. In the present work a TRACOR NORTHERN TN-1705 MCA is used.

4 EXPERIMENTAL PROCEDURE

4.1 Single Channel Analyser Window Setting

In an experiment where neutrons of energy within a specific range are to be counted, the pulses corresponding to these neutrons must be differentiated from the rest before being counted. The Single Channel Analyser is an ideal instrument to select these pulses. Figure 13 shows the schematic diagram for the counting circuitry used in the present work.

An analog pulse from the linear amplifier is split into two identical components through the 'tee' at the linear

Figure 13

Electronics for Neutron Counting

He³ DETECTOR

PREAMP ← H.V. SUPPLY

AMPLIFIER

SINGLE CHANNEL ANALYZER

SCALER

DELAY AMPLIFIER

LINEAR GATE

MCA
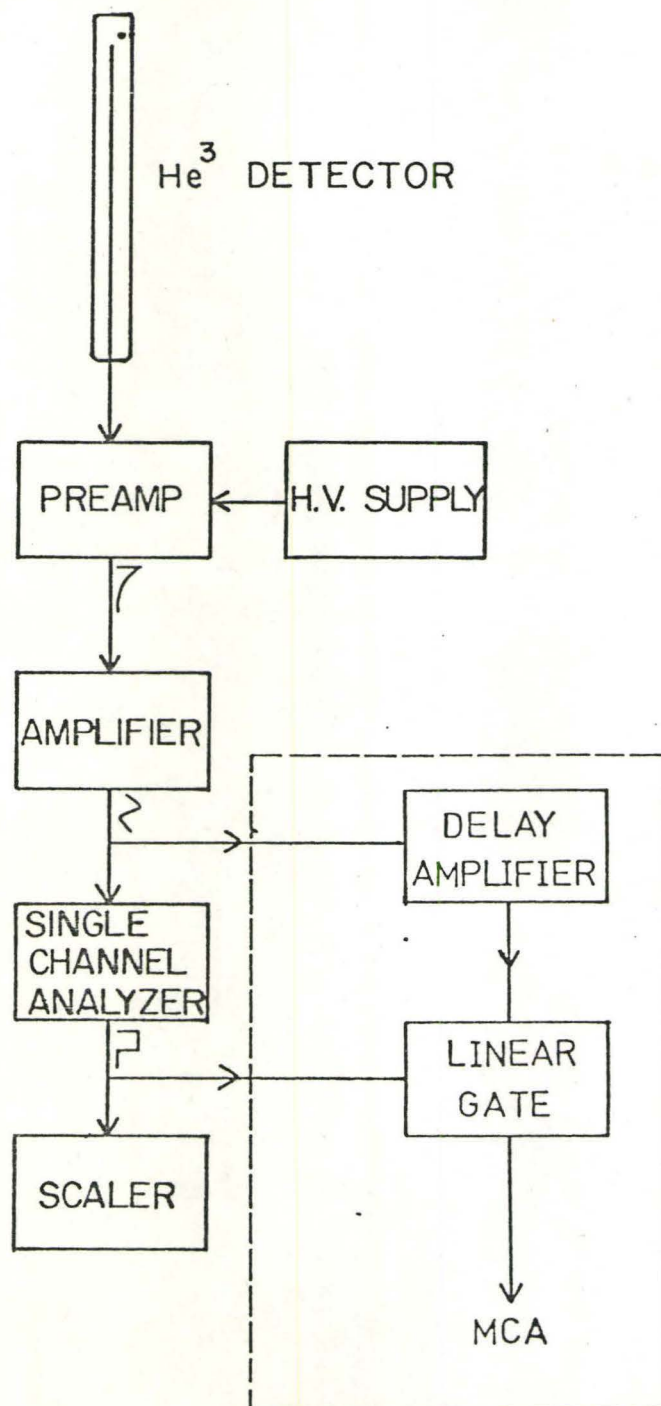
amplifier output. One component is fed through the delay amplifier and the other through the SCA with the window fully opened. The delay amplifier output signal was externally triggered by the SCA output on an oscilloscope. Delay in the delay amplifier was adjusted so that the delay amplifier and SCA output signals would emerge at the same time. After this crucial step of sychronizing the delay amplifier and the SCA outputs, the SCA logic output signal was split into two, one being fed to a scaler and the other fed into the gate input of the Linear Gate to trigger the 'gate', while the delay amplifier output signal was fed into the other input of the Linear Gate. Since both the inputs had been sychronized, the analog delay amplifier output pulse would be 'let through' the opened gate triggered by the SCA logic trigger pulse and emerge at the Linear Gate output. If the Linear Gate output is analysed by an MCA, only the part of the pulse height spectrum that falls within the SCA window may be analysed and appear in the spectrum. The other region of the pulse height spectrum will be 'wiped out'. With the window in the SCA fully opened, a self-gated neutron energy spectrum is obtained. Figure 14 shows a typical neutron spectrum obtained with the neutron beam in beam port No. 2. Region A in the spectrum is due to gamma rays. Region B is due to elastic scattering of He^3 nuclei with neutrons. Region C is the thermal/epi-thermal peak (resolution of a He^3 counter is of the order of 50 keV). Region D is due to fast neutrons.

Figure 14

Pulse Height Spectrum of Neutron Detected
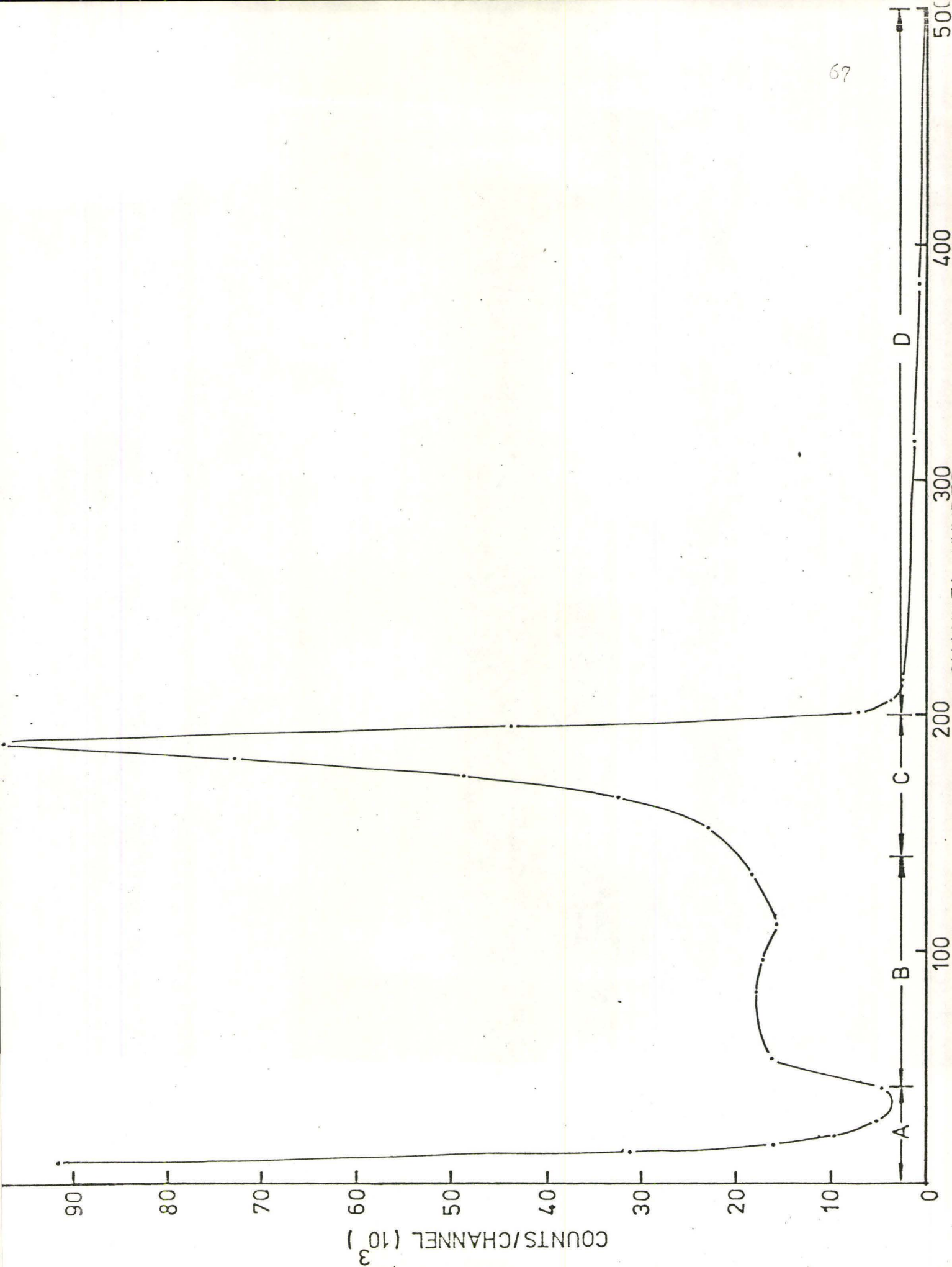
Whenever a region in the spectrum is to be gated on, e.g. the thermal/epithermal peak, the lower discriminator in the SCA is raised so that the region to the left of the region of interest no longer appears in the spectrum (analog pulses corresponding to the 'wiped out' region are grounded since the gate is not triggered as analog pulses with height below the lower discriminator cannot generate trigger pulses). The window of the SCA is then narrowed to cut off the pulses to the right of the region of interest. After the window of the SCA is set in this way, the gated spectrum will consist only of the region of interest.

After the SCA window has been set, the components in the dotted square shown in Figure 13 can be removed. The scaler will then count only pulses in the pre-set region of the pulse-height spectrum.

4.2 Beam Profile Measurement

Before the test section could be properly aligned with the beam, the beam profile must be measured, both horizontally and vertically. A sheet of cadmium 1.0 mm thick, was wrapped around the beam shutter pipe (see section 2.3) of the shutter tank to filter out thermal neutrons (Cadmium has a large total cross-section of 7500 barns at 0.2 eV while thermal neutrons have energy of 0.025 eV). The counting circuitry shown in Figure 13 was used with the SCA window set on the thermal/epithermal peak of the neutron spectrum.

The axis of a He^3 detector was aligned parallel to

the beam direction and was traversed horizontally across
the beam at intervals of 10 mm. At each interval, the number
of counts in 50 seconds was recorded. The result (horizontal
beam profile) is shown in Figure 15. Similarly, the vertical
beam profile was scanned and is shown in Figure 16.

4.3 Void Measurement by 90° Scattering for Aluminum-Water Test Section

After the beam profiles were measured, the test
section assembly (section 3.1) was lowered into the experi-
mental cavity and positioned so that the 50.8 mm specimen
holder (test section) fell into the relatively flat part of
the beam profile. The adjustment screws at the bottom of
the base frame of the assembly was adjusted so that the
axis of the He^3 counter placed in the detector sleeve was
level with the maxima of the vertical beam profile. The
rotating arm, with the He^3 detector sitting on top, was
rotated until it made an angle of 90° with the beam direction.

After this alignment was completed, the test section
would be scattering neutrons in all directions, and a He^3
detector with an effective width of 50.8 mm would detect
scattered thermal/epithermal neutrons at 90°. Figure 17
shows the schematic plan view of the experimental set-up.
Plastic bags filled with borax powder and blocks of paraffin
wax were piled around the He^3 detector to minimize background
neutron counts.

The specimen holder was first emptied and the beam
was turned on. Counts were accumulated for 200 seconds. The

Figure 15

Horizontal Beam Profile

NEUTRON COUNTING RATE
(10³ COUNTS/SEC)
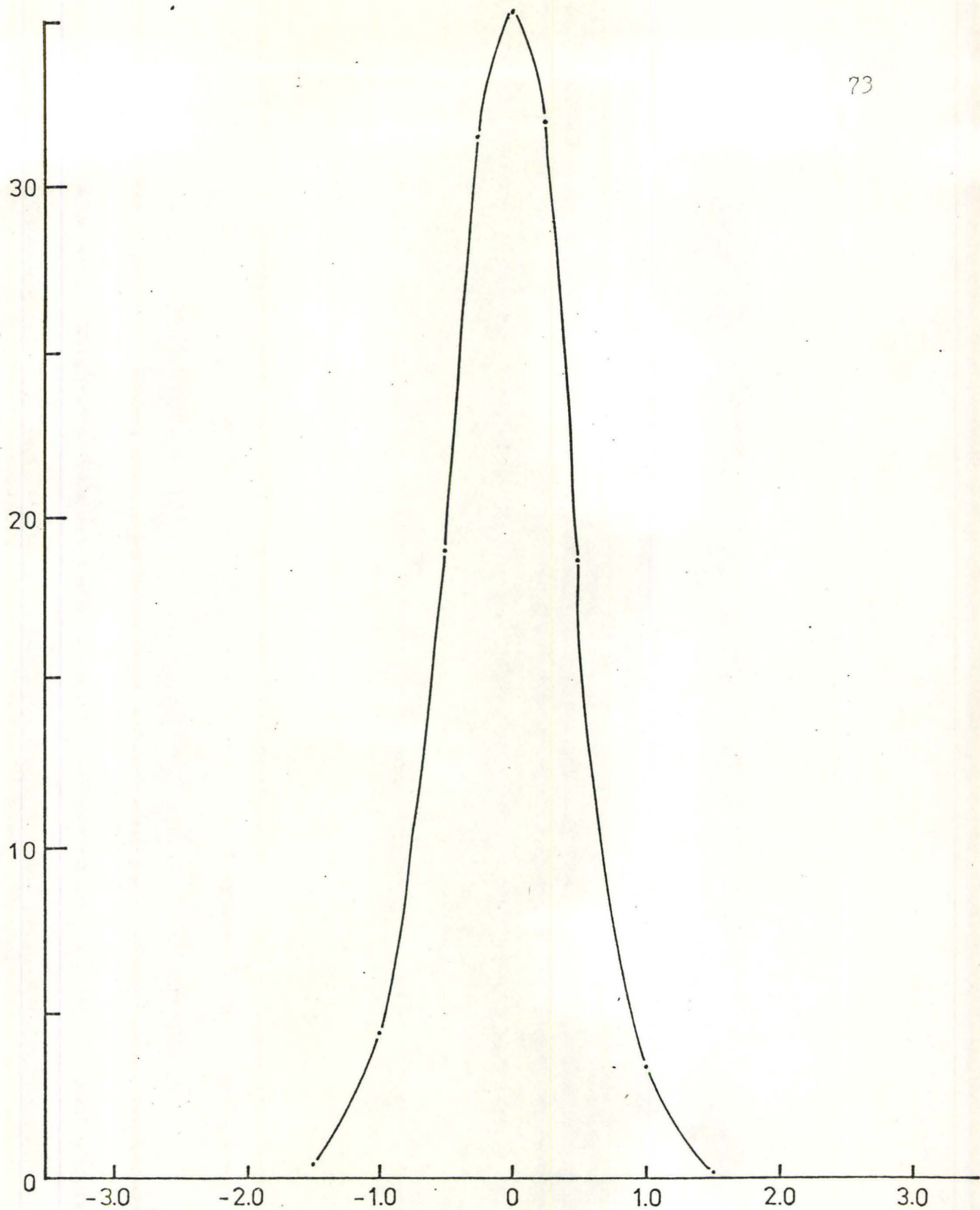
HORIZONTAL DETECTOR POSITION (25.4mm/div)

Figure 16

Vertical Beam Profile

Figure 17

Schematic Plan View of Experimental Set-up

COLLIMATED NEUTRON BEAM

Cd SCREEN

C_1

TEST SECTION

D_1

C_2
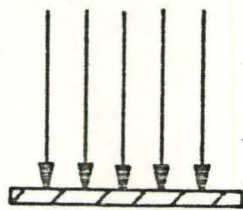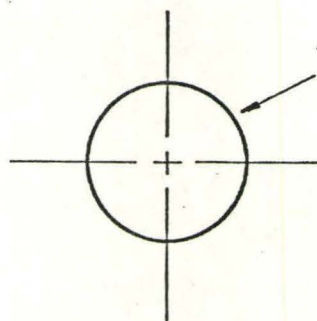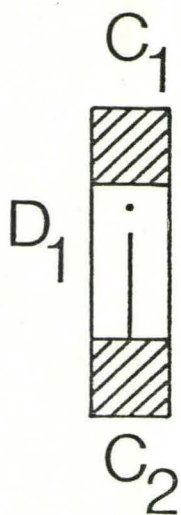
DETECTOR D_2 MAY MOVED IN THIS DIRECTION

C_1, C_2 COLLIMATORS FOR D_1

D_1 He^3 DETECTOR FOR SCATTERED FLUX

D_2 He^3 DETECTOR FOR TRANSMITTED FLUX

D_2
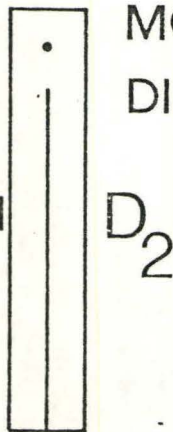
counting rate obtained, denoted by N(1), accounts for scattering due to the empty test section as well as any stray, background neutron intercepted by the He^3 detector. The specimen holder was next filled completely with water and the average scattered neutron count rate was obtained similarly. This count rate is denoted by N(0). The two quantities N(1) and N(0) are two calibration points necessary for later analyses. The specimen simulating a void of 1.0 (solid aluminum rod) was inserted into the specimen holder and an average count rate was obtained for that. This is denoted by N(1'). This quantity is useful in correcting for scattering due to aluminum specimens.

After the data for these calibration points were obtained, the experiment proceeded in a similar manner with counting being done for each specimen simulating a different void fraction α , starting with the smallest value of $\alpha = 0.25$. For each α , specimens simulating all three void distributions, namely annular, inverted annular, and stratified, were experimented with. Moreover, the same stratified specimen was rotated in four positions, namely the straight edge perpendicularly facing the beam, being on left side of the beam, perpendicularly facing away from the beam, and being on the right hand side of the beam. In this manner, for each of $\alpha = 0.25$, 0.50, 0.65, 0.75, and 0.90, six data points were obtained.

During the experiment, the reactor power might change. As a way of correcting for this power fluctuation, the

following correction step was taken for each specimen. Before the first counting and after the last counting of each set of specimens of the same void fraction inserted, the specimen holder was fully filled with water and the corresponding count rates were obtained. The average of these two values was used to normalize the average counting rate for that specimen. As the fluctuation of reactor power is a slowly varying function of time, this way of correcting for power fluctuation was found adequate.

After several sets of data were obtained (each set consists of counting rates for all specimens of all the 3 void fractions), the specimen holder was replaced with a 25.4 mm holder to accommodate a set of 25.4 mm specimens. This set of specimens consisted of ones simulating $\alpha = 0.25$, 0.50, and 0.75. Again for each void fraction the main flow regimes (annular, inverted annular, and stratified) were simulated. The He^3 counter was realigned so that the axis of the detector made an angle of 90° with the beam direction (diameter of detector is 25.6 mm). The experiment was repeated in a similar manner to obtain data for the set of 25.4 mm specimens. Also a set of data was collected using a BF_3 counter.

4.4 Identification of Flow Regimes (Neutron Transmission)

After the accumulation of data for 90° scattering was completed, the experiment moved on to determining the feasibility of identifying flow regimes by counting transmitted neutrons. In this part of the experiment, the He^3 detector

was aligned with its axis parallel to the neutron beam and level with the centroid of the beam. The detector was not shielded (as in the case of 90° scattering experiment) because the shielding material would scatter neutrons and this is not desirable. The window of the SCA was fully opened and the lower discriminator was lowered to cut off only the gamma rays. In this part of the experiment, only 50.8 mm specimens were used. The test section was filled with water and specimens simulating a given void fraction for a given distribution was inserted one at a time. For each specimen inserted, the detector was traversed across the beam at intervals of 10 mm to obtain the corresponding transmitted neutron beam profile. For a given specimen simulating a given void distribution, the profile of water path length would be different from that due to another specimen simulating the same void fraction but of different distribution. Thus, it was expected that each specimen would lead to a different neutron transmission profile.

4.5 Void Measurements for Air-Water Test Section by Neutron Scattering

After the measurements for both scattered and transmitted flux were made for the aluminum-water test section, the aluminum-water test section assembly was replaced by the air-water flow loop. The test section was aligned with the neutron beam so that the test section fell within the flat portion of the beam as in the case of the aluminum-water test section. A neutron detector was placed at the same level as the neutron beam with its axis parallel to the

beam.   The detector sleeve (see section 3.1.1) was adjusted
so that the detector is detecting scattered neutron flux at
90° with an effective detection width 38.1 mm (same dimension
as the test section).

The water pump and air supply were turned on.   The
flow rates of water and air were maintained at a steady value
to achieve a steady air-water flow in the test section.
about one minute was given to the loop to develop a steady
flow before counting of the scattered flux was started.   The
scattered flux was counted with counting time varying from
60 s to 180 s.   The two quick closing valves were closed
simultaneously to trap the air-water mixture in the test
section.   The quick closing valve V_2 at the exit side of the
test section was subsequently opened to empty the trapped
water into a measuring cylinder.   Comparing the volume of
this trapped water with the volume of the test section
between the two quick closing valves gives the volume fraction
of the water phase for this particular run.   Since the flow
was only quasi-steady, the above procedure was repeated
many times (10 to 20 times) with both air and water flow
rates maintained at the same value in order to determine the
average of the water phase fraction by trapping the water
between the quick closing valves as well as the average of
the scattered neutron flux.   The average scattered flux was
used to determine the mean void fraction in the same way as
for the aluminum-water test section.   The void fraction
determined by neutron scattering was then compared with that

determined by trapping water between the quick closing valves.

The above procedure was repeated for the entire range of void between 0 and 1.0.

5 ANALYSES, RESULTS, AND DISCUSSIONS

5.1 Void Fraction Determined by Neutron Scattering

One of the main objectives of the present work was to determine how the scattered flux is related to void fraction. Based on the hypothesis that the scattered flux is proportional to the amount of water in the test section and that the scattered flux is independent of the distribution of the water distribution, the volume fraction of water in the test section, α'_E, is given by

$$\alpha'_E = [N(\alpha) - N(1)] / [N(0) - N(1)] \tag{15}$$

where $N(0)$ = scattered neutron count rate at void fraction 0.0.

$N(1)$ = scattered neutron count rate at void fraction 1.0

$N(\alpha)$ = scattered neutron count rate at void fraction α. (This quantity is corrected for scattering due to the aluminum specimen in the case of the aluminum-water test section assuming that the contribution due to aluminum is proportional to α and is given by $\alpha N(1')$

Hence, the void fraction occupied by the aluminum specimen, α_E, is then

$$\alpha_E = 1 - \alpha'_E$$

$$= [N(0) - N(\alpha)] / [N(0) - N(1)] \tag{16}$$

To test the assumption that the scattered flux is independent of void distribution and proportional to the amount of hydrogeneous material, the void fraction determined by neutron scattering, α_E, was plotted against the actual void fraction. The actual void fraction was either that occupied by the aluminum specimen in the aluminum-water tests or the average void fraction occupied by air determined by trapping water between the quick closing valves in the air-water tests. If equation (16) is correct then the actual and calculated void fractions should agree.

5.1.1 Results for Aluminum-Water Test Section

Results obtained from the scattered neutron measurements with the 25.4 mm aluminum-water test section are shown in Figure 13 and the corresponding data are shown in Appendix A1.1.1. A sample data analysis and error analysis are given in Appendices A3.1 and A4.1.1 respectively. The position of the beam, test section and counter are shown in the insert to the figure. From the figure it is evident that there is a difference between measurements for the stratified patterns. If the aluminum (i.e. the void) is closer to the counter, the detector 'sees' less scattered neutrons than when the aluminum (void) is further away. Hence, the void fraction determined when the aluminum is closer to the detector is higher than the actual value. On the other hand when the aluminum is further away, the detector 'sees' more scattered neutrons and the void fraction thus determined is lower. This effect can be compensated for by positioning two detectors opposite each

Figure 18

Correlation between Void Fraction determined by Neutron Scattering and Actual Void Fraction in 25.4 mm Aluminum-Water Test Section

ANNULAR
INVERTED ANNULAR
STRATIFIED 1
" 2
" 3

SCHEMATIC   STRATIFIED
PATTERN   POSITIONING

BEAM → WATER
Al

He³ DETECTOR

VOID FRACTION FROM NEUTRON SCATTERING

ACTUAL VOID FRACTION
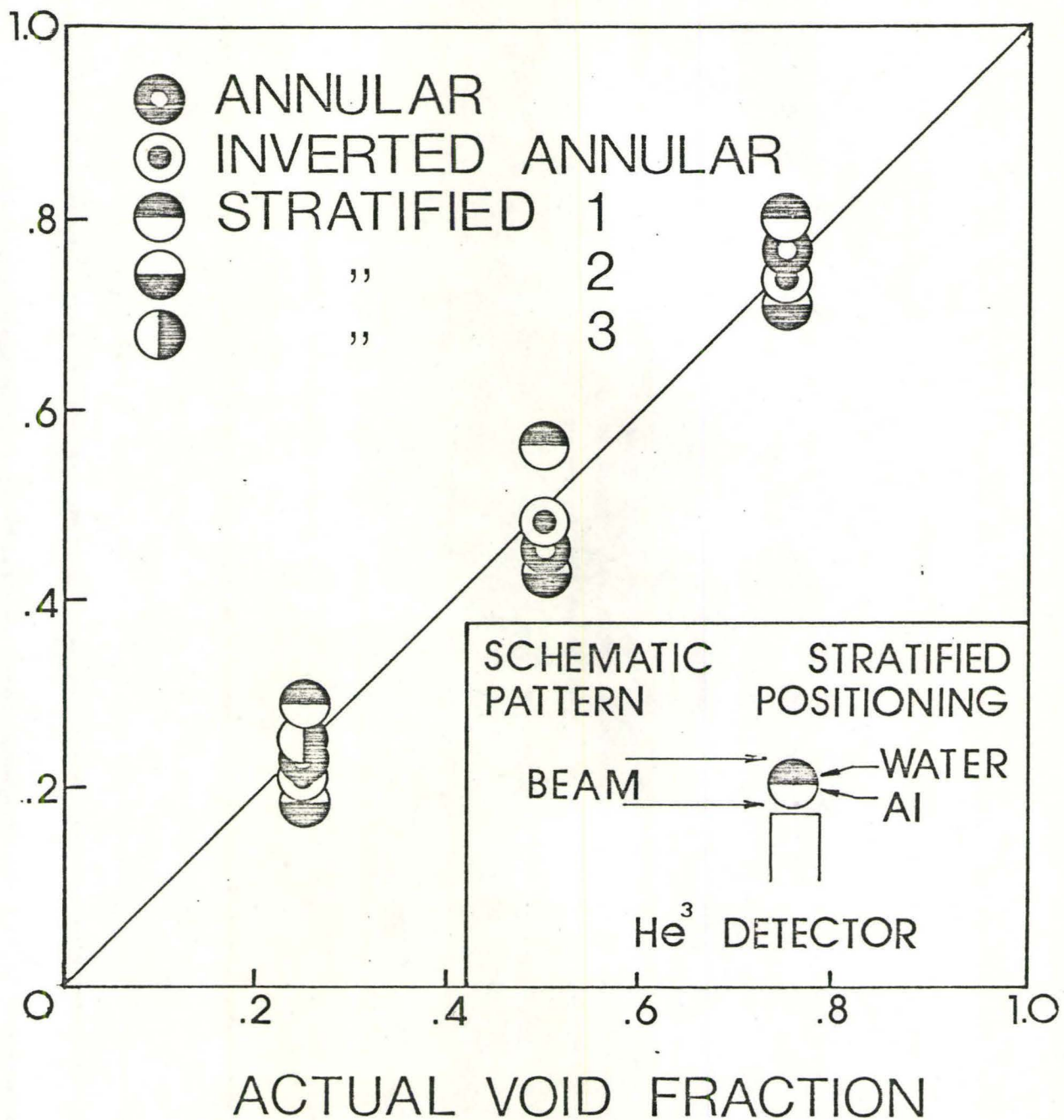
other and averaging the count rates.

Apart from the effect mentioned above, the data points do fall closely into a straight line indicating that equation (16) is reasonably accurate.

Figure 19 shows the experimental results for the 50.8 mm test section and the corresponding data are presented in Appendix A1.1.2. The effect of water distribution in stratified flow on experimentally determined void fraction is again evident and is somewhat accentuated. Again, the effect can be compensated for by averaging the count rates from two counters placed opposite each other. The annular and inverted annular water distributions also lead to values of α_E's which are slightly lower than the actual void fraction.

Apart from slight deviation from the linear behaviour of the results from the scattering experiments as shown in Figures 18 and 19, equation (16) is reasonably accurate. The fast neutron scattering technique is evidently quite promising for measuring void fractions.

5.1.2 Results for Air-Water Tests

Results for the air-water tests are shown in Figure 20. The corresponding data are presented in Appendix A1.2. Sample data analyses and error analyses are given in Appendices A3.2 and A4.1.2 respectively.

The void fraction measured by trapping water between quick closing valves is an average of several measurements. Especially in slug flow, the amount of water trapped varied by a considerable amount and the average void fraction was

Figure 19

Correlation between Void Fraction determined by Neutron
Scattering and Actual Void Fraction in 50.8 mm Aluminum-
Water Test Section
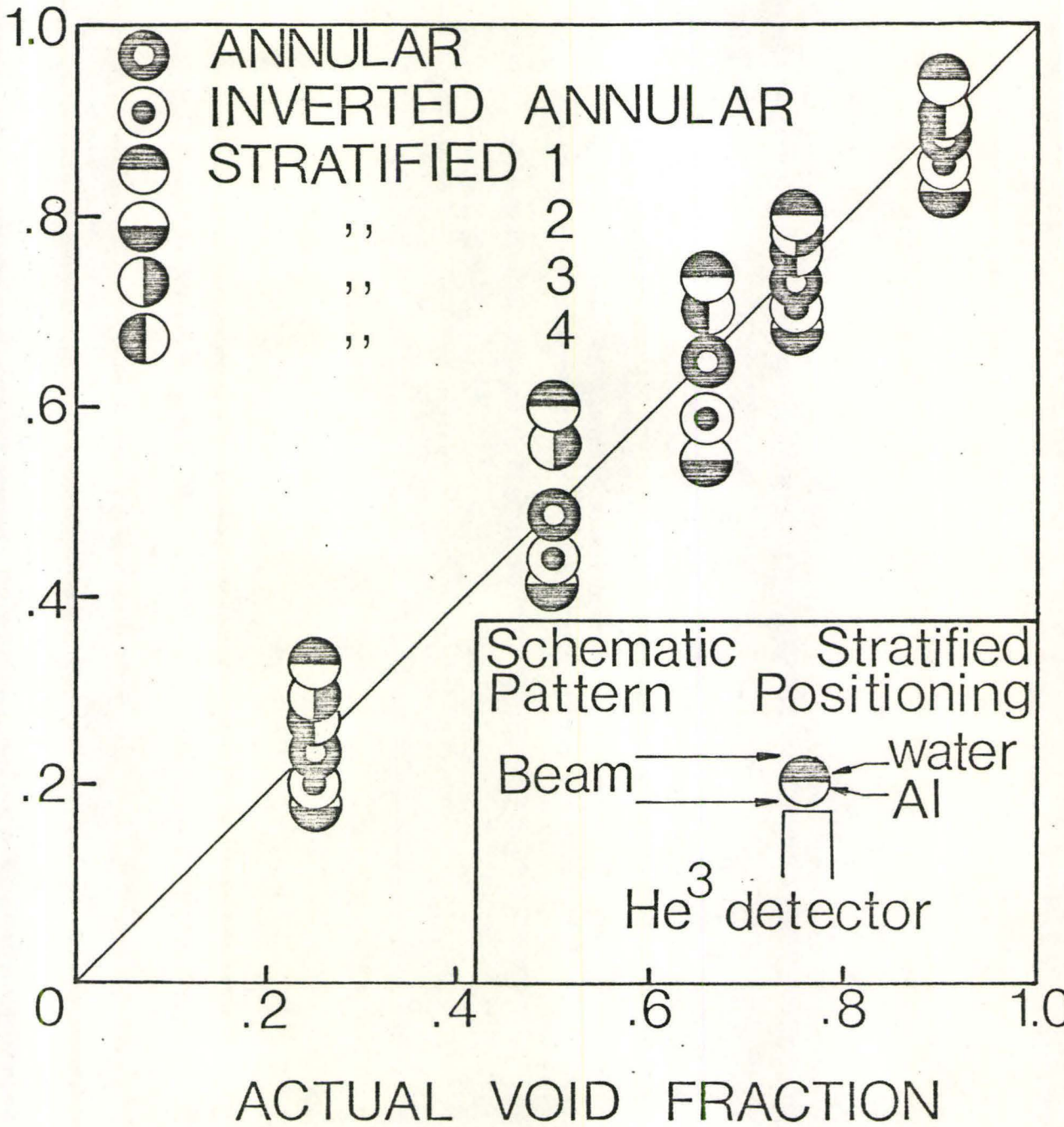
obtained from fifteen to **twenty** measurements. The void fraction determined by the scattered neutron flux was obtained by averaging the count rate over 60 to 180 seconds. This averaging was done for the purposes of comparison with the ensemble averaged quick closing valve measurements.

It can be observed from Figure 20 that the data points fall closely into a straight line with the exception of two points. Also, the neutron scattering method gives a void fraction slightly lower than obtained by the quick closing valve technique as shown in the figure. These results are similar to those obtained for the aluminum-water test section indicating that this technique of measuring average void fraction is very promising.

5.2 Flow Pattern Identification

In order to test the feasibility of identifying flow regimes by measurement of transmitted neutrons, the transmitted neutron flux through each 50.8 mm specimen was scanned at intervals of 10 mm with He^3 detector as described previously. The purpose was to determine whether different void distributions (different water path-length profiles) would lead to different attenuation of the beam resulting in different transmitted beam profiles. The results are shown in Figures 21, 22, 23, and 24. Figure 21 shows the transmitted flux across the 50.8 mm test section full of water ($\alpha = 0$). The transmitted beam profile is not entirely flat, so the counts

Figure 20

Correlation between Void Fraction determined by Neutron

Scattering and Void Fraction determined by Trapping Water

in the Air-Water Test Section
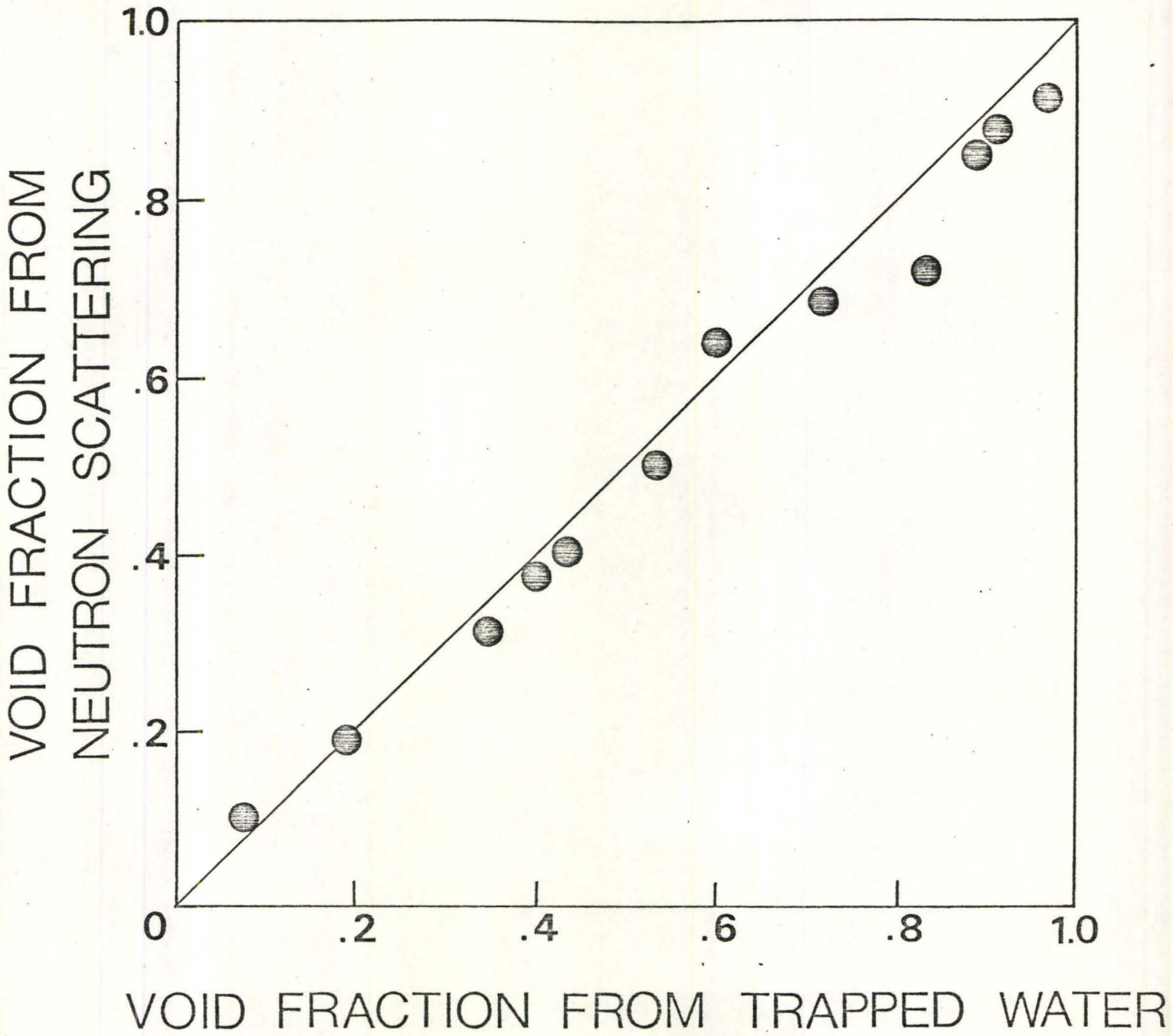
Figure 21

Transmitted Beam Profile for Full Test Section
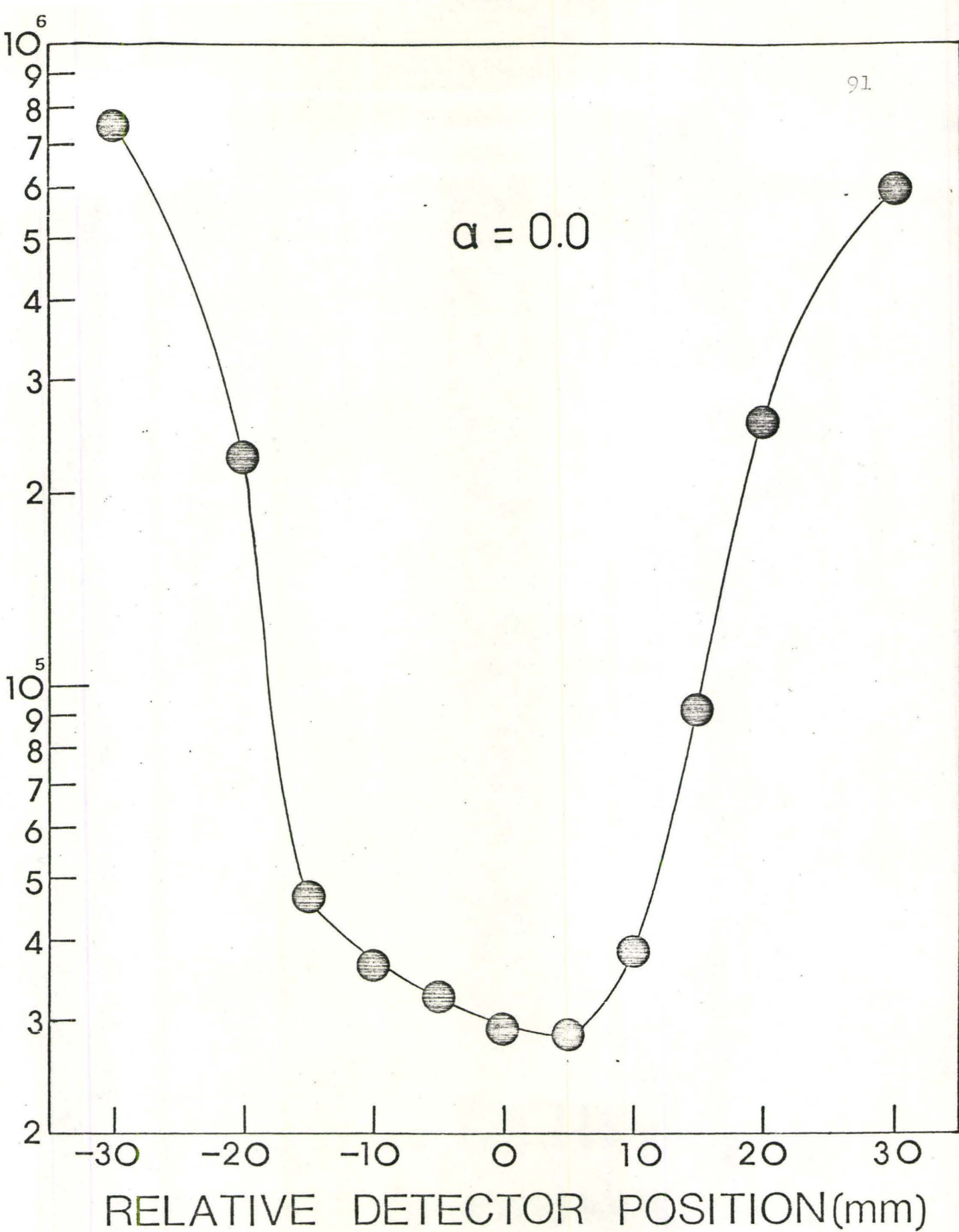
are not exactly symmetric. However, it is evident that the transmitted flux is attenuated by more than an order of magnitude by the presence of water.

The way in which the transmitted beam profile changes with flow pattern at a low void fraction ($\alpha = 0.25$) is shown in Figure 22. The stratified flow pattern was such that the void was on the left hand side and the water on the right hand side. Even at these low void fractions, the difference between the various flow patterns is clear. Annular patterns give rise to a characteristic double humped profile. Stratified patterns give a highly asymmetric profile and inverted annular patterns give a symmetric profile with attenuation in the middle. In Figure 23 these characteristic profile repeat themselves and become more distinct from one another as the void fraction is increased to $\alpha = 0.50$. In Figure 24, we can see that the characteristic profiles are further accentuated at the higher void fraction of $\alpha = 0.75$. The differences between the flux profiles for the various simulated flow patterns are very large at the higher void fractions.

6 CONCLUSIONS

From the experimental results presented above, the following conclusions may be drawn.

(i)   The scattered flux is not entirely independent of the void distribution as can be shown from the results for stratified void distribution.

(ii)   In general, it appears that if two counters are used

Figure 22

Transmitted Beam Profile for 25 % Voided Test Section with
Simulated Annular, Inverted Annular, and Stratified Flow
Regimes
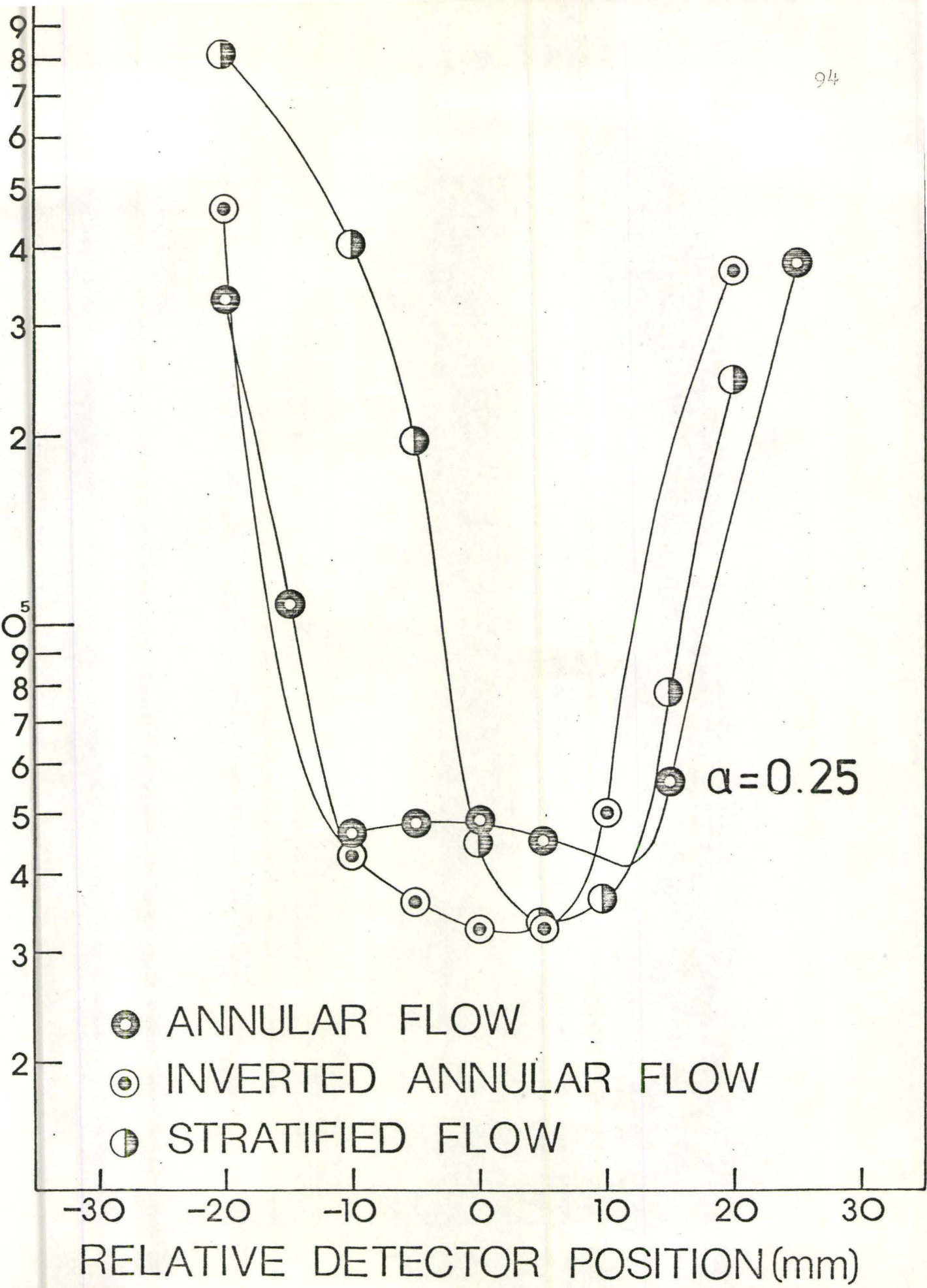
Figure 23

Transmitted Beam Profiles for 50 % Voided Test Section with
Simulated Annular, Inverted Annular, and Stratified Flow
Regimes

96
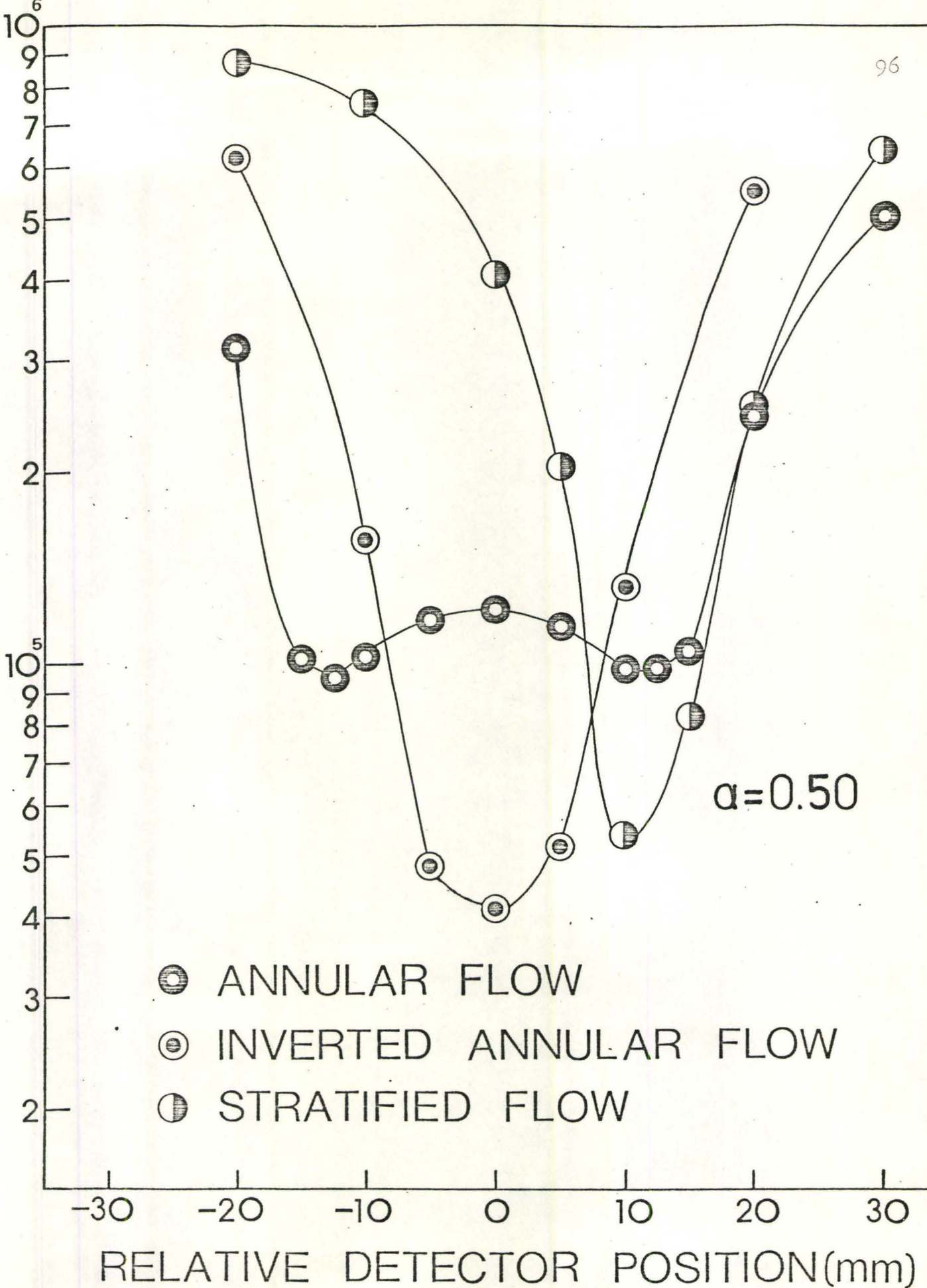
Figure 24

Transmitted Beam Profile for 75 % Voided Test Section with
Simulated Annular, Inverted Annular, and Stratified Flow
Regimes
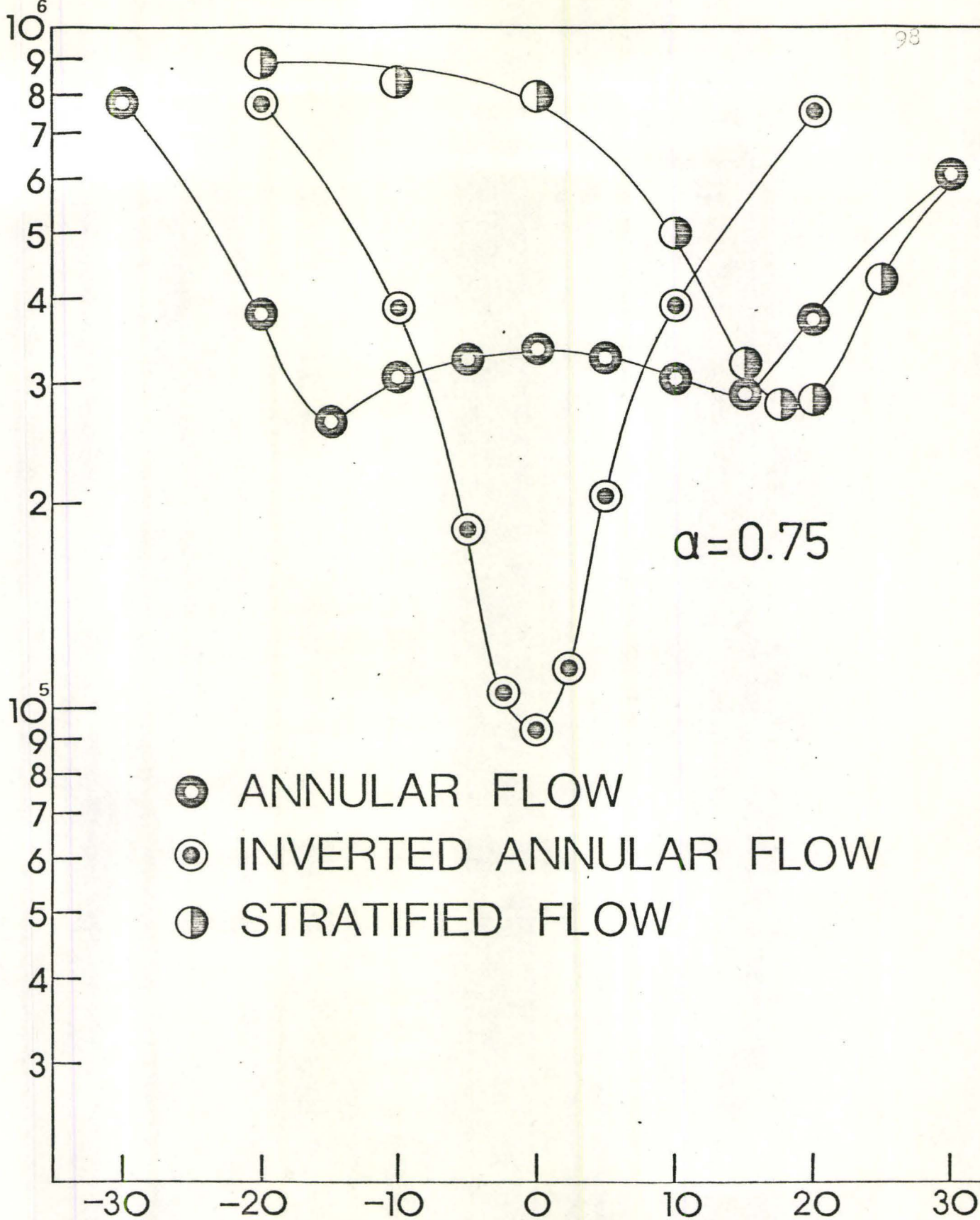
α = 0.75

to measure the scattered flux and the count rates are averaged, then the technique will lead to void fractions which are close to the actual values, though perhaps slightly low.

(iii) The agreement of the void fractions between the trapped water method and the neutron scattering method is sufficiently good that the neutron scattering technique may be used as a reference for calibrating other types of densitometers.

(iv) Measurements of the transmitted flux indicate with good sensitivity the main flow patterns, at least in the aluminum-water simulations.

APPENDIX

A1 DATA FOR VOID MEASUREMENT BY NEUTRON SCATTERING

Scattered neutron flux readings and the void fractions determined from such readings are reported for both the aluminum-water test section and the air-water test section in the following subsections. A sample data analysis is given in Appendix A3.1 and a sample error analysis for the associated error reported in the subsequent sections is given in A4.1. Errors quoted in data tables are 'one standard errors', i.e. 68% confidence level.

A1.1 Aluminum-Water Test Section

In the following tables, different flow regimes are designated by a code number as shown in the following:

Flow Regime	Code	Configuration*
Annular	1	
Inverted Annular	2	
Stratified 1	3	
Stratified 2	4	
Stratified 3	5	
Stratified 4	6	

---

* See relative detector positioning on Figures 18 and 19.

A1.1.1 Aluminum-Water Test Section of 25.4 mm

(a) Run No. 1

Counting Time: 100 s

Actual Void	Flow Regime	Counts of Scattered Neutrons	Void Fraction
0.		95919	
0.25 ± 0.01	1	78798	0.23 ± 0.04
	2	79992	0.21 ± 0.04
	3	73305	0.29 ± 0.04
	4	76486	0.25 ± 0.04
	6	80490	0.21 ± 0.04
0.50 ± 0.01	1	59294	0.48 ± 0.04
	2	58482	0.49 ± 0.04
	3	52599	0.56 ± 0.04
	6	59952	0.47 ± 0.04
0.75 ± 0.01	1	37283	0.76 ± 0.04
	2	38939	0.75 ± 0.04
	3	33676	0.81 ± 0.04
	6	39156	0.74 ± 0.04
1.0	air	11145	
	aluminum	19432	

(b) Run No. 2

Counting Time: 100 s

Actual Void	Flow Regime	Counts of Scattered Neutrons	Void Fraction
0.0		90135	
0.25 ± 0.01	1	73305	0.23 ± 0.03
	2	73951	0.22 ± 0.03
	3	76993	0.29 ± 0.03
	4	72229	0.24 ± 0.03
	6	75203	0.21 ± 0.03
0.50 ± 0.01	1	55611	0.47 ± 0.04
	2	56071	0.47 ± 0.04
	3	49289	0.55 ± 0.04
	4	54147	0.49 ± 0.04
	6	56702	0.46 ± 0.04
0.75 ± 0.01	1	36064	0.74 ± 0.03
	2	35968	0.74 ± 0.03
	3	32383	0.73 ± 0.03
	4	34908	0.75 ± 0.03
	6	37114	0.72 ± 0.03
1.0	air	9539	
	aluminum	16669	

(c) Run No. 3

Counting Time: 100 s

Actual Void	Flow Regime	Counts of Scattered Neutrons	Void Fraction
0.0	1	98326	0.20 ± 0.05
0.25 ± 0.01	2	87430	0.19 ± 0.05
	3	83073	0.27 ± 0.05
	4	85293	0.23 ± 0.05
	6	87661	0.20 ± 0.05
0.50 ± 0.01	1	73270	0.45 ± 0.05
	2	71870	0.48 ± 0.05
	3	68147	0.53 ± 0.05
	4	71798	0.48 ± 0.05
	6	73101	0.46 ± 0.05
0.75 ± 0.01	1	58061	0.72 ± 0.05
	2	59273	0.70 ± 0.05
	3	53863	0.79 ± 0.05
	4	58778	0.71 ± 0.05
	6	58344	0.72 ± 0.05
1.0	air	33839	
	aluminum	42147	

A1.1.2 Aluminum-Water Test Section of 50.8 mm

(a) Run No. 1

Counting **Time:** 200 s

Actual Void	Flow Regime	Counts of Scattered Neutrons	Void Fraction
0.0		104181	
0.25 ± 0.01	1	85460	0.23 ± 0.03
	2	87850	0.21 ± 0.03
	3	76692	0.32 ± 0.03
	4	82141	0.26 ± 0.03
	5	83210	0.25 ± 0.03
	6	90234	0.17 ± 0.03
0.50 ± 0.01	1	63535	0.49 ± 0.03
	2	67712	0.44 ± 0.03
	3	53416	0.60 ± 0.03
	4	57548	0.55 ± 0.03
	5	61622	0.51 ± 0.03
	6	72068	0.39 ± 0.03
0.75 ± 0.01	1	41190	0.75 ± 0.03
	2	43730	0.72 ± 0.03
	3	32368	0.85 ± 0.03
	4	37472	0.79 ± 0.03
	5	39784	0.76 ± 0.03
	6	46316	0.69 ± 0.03
1.0	air	13334	
	aluminum	20118	

(b) Run No. 2

Counting Time: 200 s

Actual Void	Flow Regime	Counts of Scattered Neutrons	Void Fractions
0.0		103723	
0.25 ± 0.01	1	85697	0.22 ± 0.03
	2	87323	0.20 ± 0.03
0.50 ± 0.01	1	66440	0.45 ± 0.03
	2	66137	0.45 ± 0.03
0.65 ± 0.01	1	54830	0.59 ± 0.03
	2	54350	0.60 ± 0.03
	3	42450	0.72 ± 0.03
	4	44863	0.70 ± 0.03
	5	51447	0.63 ± 0.03
	6	60453	0.53 ± 0.03
0.75 ± 0.01	1	45237	0.70 ± 0.03
	2	44303	0.71 ± 0.03
0.90 ± 0.01	1	32200	0.86 ± 0.03
	2	30667	0.86 ± 0.03
	3	25990	0.93 ± 0.03
	4	26940	0.92 ± 0.03
	5	31033	0.87 ± 0.03
	6	32233	0.86 ± 0.03
1.0	air	10810	
	aluminum	19263	

Al.2 Air-Water Test Section

Several runs were completed to investigate the feasibility of the technique of neutron scattering in measuring void in an air-water test section. Results shown in Figure 20 are the composite of these runs.

(a) Run No. 1

Counting Time: 60 s

Average Volume of Trapped Water (ml)	Average Void from Trapped Water	Average Scattered Neutron Counts	Void Fraction from Neutron Scattering
669 ± 7	0.0	10554 ± 661	
310 ± 66	0.54 ± 0.12	6799 ± 354	0.52 ± 0.12
266 ± 39	0.60 ± 0.09	5884 ± 98	0.65 ± 0.11
115 ± 5	0.83 ± 0.04	5310 ± 66	0.73 ± 0.12
194 ± 27	0.71 ± 0.10	5535 ± 119	0.70 ± 0.12
0	1.0	3342 ± 296	

(b) Run No. 2

Counting Time: 180 s

Average Volume of Tapped Water (ml)	Average Void from Trapped Water	Average Scattered Neutron Counts	Void Fraction from Neutron Scattering
669 ± 7	0.0	11026 ± 114	
535 ± 12	0.20 ± 0.01	9316 ± 85	0.19 ± 0.02
428 ± 8	0.36 ± 0.01	8200 ± 131	0.31 ± 0.02
390 ± 12	0.42 ± 0.01	7539 ± 64	0.39 ± 0.02
378 ± 21	0.43 ± 0.02	7408 ± 57	0.40 ± 0.02
612 ± 4	0.09 ± 0.00	10159 ± 52	0.10 ± 0.02
0	1.0	3017 ± 70	

(c) Run No. 3

Counting Time 60 s

Average Volume of Trapped Water (ml)	Average Void from Trapped Water	Average Scattered Neutron Counts	Void Fraction from Neutron Scattering
669 ± 7	0.0	11026 ± 114	
535 ± 12	0.20 ± 0.01	9316 ± 85	0.19 ± 0.02
428 ± 8	0.36 ± 0.01	8216 ± 131	0.31 ± 0.02
390 ± 12	0.42 ± 0.01	7539 ± 64	0.39 ± 0.02
378 ± 21	0.43 ± 0.02	7408 ± 57	0.40 ± 0.02
612 ± 4	0.09 ± 0.00	10159 ± 52	0.10 ± 0.02
0	1.0	2017 ± 70	

A2 DATA FOR MEASUREMENT OF TRANSMITTED BEAM PROFILE

In this run, the axis of the He^3 detector was parallel to that of the neutron beam and the detector was traversed across the beam profile at intervals of 10 mm each. Stratified flow regimes in the following tabulated data means that the aluminum (void) is on the left and thus the water is on the right from the view of the detector looking directing at the beam. The counting time for each scanning position is 30 s.

(a) α = 0.0

Relative Detector Position (10 mm)	Counts
-3.0	742190
-2.0	224120
-1.5	46708
-1.0	36326

(a) Continued

Relative Detector Position (10 mm)	Counts
-0.5	32369
0.0	28396
0.5	28374
1.0	38326
1.5	91078
2.0	255378
3.0	591193

(b) $\alpha = 25$ %

Relative Detector Position (10 mm)	Annular Flow	Inverted Annular Flow	Stratified Flow
-2.0	327390	458724	806340
-1.5	113926		
-1.0	46453	42874	402645
-0.5	48271	36118	192427
0.0	48248	32767	44619
0.5	44684	32498	33081
1.0		50043	36517
1.5	56364		77664
2.0		362454	242786
2.5	373912		

(c) α = 50 %

Relative Detector Position (10 mm)	Annular Flow	Inverted Annular Flow	Stratified Flow
-2.0	311097	618157	871682
-1.5	101445		
-1.25	94820		
-1.0	102527	156451	758008
-0.5	116758	48005	
0.0	120590	41297	407279
0.5	114288	51395	203981
1.0	98029	131996	54102
1.25	98615		
1.5	104730		83921
2.0	242631	542459	253292
3.0	550223		636724

(d) α = 75 %

Relative Detector Position (10 mm)	Annular Flow	Inverted Annular Flow	Stratified Flow
-3.0	774384		
-2.0	376935	766747	870134
-1.5	261694		
-1.0	303039	384099	814821
-0.5	324662	173327	
-0.25		108246	
0.0	333416	92343	788766
0.25		124965	
0.5	327108	203242	

(d) Continued

Relative Detector Position (10 mm)	Annular Flow	Inverted Annular Flow	Stratified Flow
1.0	303333	388742	496554
1.5	288744		319997
1.75			279858
2.0	370627	740868	280419
2.5			422219
3.0	602121		588231

A3 SAMPLE DATA ANALYSES

A3.1 Aluminum-Water Test Section

The data analysis for the data point of simulated annular flow with $\alpha = 0.25$ in run No.1 of 25.4 mm aluminum-water section is given as a sample.

It was found that the reactor power did not fluctuate for more than 1.0 %. There was thus no need to correct the counts of scattered neutrons for the power fluctuation.

From the table in A1.1.1 (a), useful data are shown as the following:

$N(0) = 95919$

$N(1) = 11145$

$N(1') = 19432$

$n(.25) = 78798$

where $N(0)$ = counts of scattered neutron when the test section is full of water ($\alpha = 0$).

$N(1)$ = counts of scattered neutrons when the test section is filled with air ($\alpha = 1$).

$N(1')$ = counts of scattered neutrons when the test section is filled with the aluminum specimen simulating air and a void of 1.0

$N(0.25)$ = counts of scattered neutrons for $\alpha = 0.25$ without correcting for aluminum scattering.

It can be observed that aluminum does scatter neutrons to a certain extent, i.e. $N(1) \neq N(1')$. In order to correct for scattering due to aluminum in the specimen simulating the void, it is assumed, to the first approximation, that the amount of scattering is proportional to the amount of aluminum. Hence, the number of scattered neutrons corrected for aluminum scattering, $N(0.25)$, is then given by

$$N(\alpha) = n(\alpha) - \left[N(1') - N(1)\right]\alpha$$

$$\therefore N(0.25) = n(0.25) - \left[N(1') - N(1)\right] \cdot 0.25$$

$$= 78798 - (19432 - 11145) \times 0.25$$

$$= 78798 - 2072$$

$$= 76726$$

To determine void fraction from neutron scattering, use equation 16,

$$\alpha_E = \frac{N(0) - N(\alpha)}{N(0) - N(1)}$$

$$= (95919 - 76726)/(95919 - 11145)$$

$$= 0.23$$

The same procedure hold for all data points in the runs fro the 25.4 mm as 50.8 mm test section.

A3.2 Air-Water Test Section

The analysis for the first data point in Run No. 1 for the air-water test section is given as a sample.

The void fraction was measured by (i) trapping the

water between the two quick-closing valves, and (ii) by neutron scattering method.

(i) Trapping Water:

The volume of water trapped in 10 trials are listed as 433, 380, 312, 338, 260, 256, 223, 238, 331, and 329 ml. The average volume $\bar{V}$ is then

$$\bar{V} = \sum_{i=1}^{10} V_i/10$$
$$= 310 \text{ ml}.$$

Since the volume of water in a full test section is 669 ml, the void fraction measured by trapping the water, is then

$$\bar{V} = 1 - 310/669$$
$$= 0.54$$

(ii) Neutron Scattering

Corresponding scattered neutron counts for the 10 trappings are 6518, 7151, 7007, 6989, 6331, 7102, 6845, 6658, 6452, 6938. The average counts over each counting interval, $\bar{N}$ is then

$$\bar{N} = \sum_{i=1}^{10} N_i / 10$$
$$= 6799$$

The average counts for a full and empty test $N(0)$ and $N(1)$ were obtained in similar manner and were found to be 10554 and 3342 respectively.

Using equation 16, void fraction measured using neutron scattering is obtained as

$$\alpha = \frac{N(0) - N(\alpha)}{N(0) - N(1)}$$

$$= (10554 - 6799)/(10554 - 3342)$$

$$= 0.52$$

The above procedure of analyses hold for other data points in all runs for the air-water test section.

A4 ERROR ANALYSIS

Possible errors for counting rates include the fluctuation of reactor power, positioning error, and statistical fluctuation in counting rate.

Reactor power may fluctuate during the course of the experiment, especially if the experiment is performed within a few hours after reator start-up. However, the present work was done at relatively stable reactor power. On checking with the power monitor chart at the reactor control room, it was found that the reactor power did not fluctuate more than 1 %. This was also confirmed by the reactor power monitor counting rate obtained (frequent checkings for full test section counting rate). Thus, a 1 % error was placed as an uppper limit on the error due to reactor power fluctuation.

Since the beam width was larger than the diameter of the test section (see the beam profile in Figure 15), the error associated with misalignment of the test section with the beam is negligible. The only error arising from positioning is the misalignment of the 90° detector with the test section. An upper limit of 0.5 mm was placed on the detection width of the detector owing to misalignment. To the first approximation, it is reasonable to assume that the counting rate is proportional to the detection width of the detector. Thus, the error is then about 2 % for 25.4 mm test section

and 1 % for 50.8 mm test section.

For the aluminum-water test section, the error due to statistical fluctuation is given by the usual $\sqrt{N}$ estimate. For the air-water test section, the mean of count rate readings for the same void created was taken. The root-mean-square deviation (one standard deviation) was taken as the error of the count rate given by (46):

$$E = (\sum_{i=1}^{N} (R_i - \bar{R})^2 / (N - 1))^{\frac{1}{2}}$$

where   E = statistical error

R$_i$ = count rate of ith trial

N = number of trials

The error associated with the linear dimension in the machined aluminum species is estimated to be 5×10^{-2} mm. The error of the mean of volume of trapped water is again the standard deviation from the mean. A sample error analysis is given both the aluminum-water and air-water test section.

A4.1.1 Aluminum-Water Test Section

The error analysis for the data point of 25 % void, annular flow given in Run No. 1 of 25.4 mm test section is presented as a sample.

Error in linear dimension of the specimen is 0.05 mm.

The simulated void, α is given by

$$\alpha = \pi(R^2 - r^2) / \pi R^2$$

$$= 1 - (r/R)^2$$

where   r = radius of specimen

R = ID of specimen holder

The error $\Delta\alpha$ is then given by

$$\Delta\alpha = \Delta(r/R)^2$$
$$(r/R)^2\left\{\sqrt{2(\Delta r/r)^2 + 2(\Delta R/R)^2}\right\}$$

with $\quad \Delta r = \Delta R = 0.05$ mm

$\qquad r = 6.35$ mm

$\qquad R = 12.7$ mm

$\quad (r/R)^2 = 0.250$

Thus $\quad \Delta\alpha = 0.250 \pm 0.003$

It can thus be seen that an error of 0.01 can be put as an upper limit on the error of the known simulated void.

The error in the scattered neutron counts is a composite of those due to reactor fluctuation (1 %), position (2 %), and statistical fluctuation ($1/\sqrt{N}$). Thus, the relative error in the scattered neutron counts uncorrected for aluminum scattering is given by

$$\frac{\Delta N'}{N'} = \sqrt{(0.01)^2 + (0.02)^2 + (1/\sqrt{78798})^2}$$

$$= 0.023$$

Similarly, relative error for $N(0)$, $N(1)$, and $N(1')$ are found to be 0.023, 0.024, and 0.023 respectively.

The scattered neutron counts corrected for scattering due to aluminum is given by

$$N(\alpha) = N'(\alpha) - \alpha(N(1') - N(1))$$

Hence, $\quad \Delta N(\alpha) = \left[(\Delta N')^2 + \alpha^2 \Delta(N(1') - N(1))^2\right]^{1/2}$

$$= \left\{(0.023 \times 78798)^2 + (0.25)^2[(0.023 \times 19432)^2 + (0.024 \times 11145)^2]\right\}^{1/2}$$

$$= 1817$$

Since $\quad \alpha_E = \dfrac{N(0) - N(\alpha)}{N(0) - N(1)}$

then $\quad \Delta\alpha_E / \alpha_E = \left\{ \left[\dfrac{\Delta(N(0) - N(\alpha))}{(N(0) - N(\alpha))} \right]^2 + \left[\dfrac{\Delta(N(0) - N(1))}{(N(0) - N(1))} \right]^2 \right\}^{1/2}$

$= \left\{ \dfrac{(0.023 \times 95919)^2 + 1817^2}{(95919 - 78798)^2} + \dfrac{(0.023 \times 95919)^2 + (0.024 \times 11145)^2}{(95919 - 11145)^2} \right\}^{1/2}$

$= 0.17$

or $\quad \alpha_E \quad = 0.23 \pm 0.04$

A4.1.2 Air-Water Test Section

The error analysis for the data point of 54 % void in Run No. 1 for the air-water test section is given as a sample error analysis.

The readings of volume of trapped water for 10 trials are listed as 433, 380, 312, 338, 260, 256, 223, 238, 331, and 329 ml. Hence, the mean volume of trapped water $\overline{V}$ is given by

$$\overline{V} = \sum_{i=1}^{N} V_i \, / \, N$$

$= (433 + 380 + 312 + 338 + 260 + 256 + 223 + 238 + 331 + 329)/10$

$= 310$

and $\quad \Delta V = \left\{ \displaystyle\sum_{i=1}^{N} (V_i - \overline{V})^2 \, / \, (N - 1) \right\}^{\frac{1}{2}}$

$= \left\{ \displaystyle\sum_{i=1}^{N} (V_i - 310)^2 \, / \, 9 \right\}^{\frac{1}{2}}$

$= \quad 66$

The readings of scattered neutron counts corresponding to these 10 trials are 6518, 7151, 7007, 6989, 6331, 7102, 6845, 6658, 6452, and 6938. In similar manner, using the standard deviation as the error in the counts, the scattered

neutron counts, $\overline{N}(\alpha)$ is given as

$$\overline{N}(\alpha) = 6799 \pm 354$$

Taking $N(0)$ and $N(1)$ as 10554 ± 661 and 3342 ± 296 respectively, the void fraction determined by neutron scattering α_E is found to be

$$\alpha = 0.52 \pm 0.12$$

A4.2 Neutron Transmission Measurement

The error for each reading of transmitted neutron counts is taken as $\sqrt{N}$. Since the counts are of the order of 10^5, the percentage errors are of the order of 0.3 % and is negligible.

REFERENCES

1. Hewitt, G.F. and Lovegrove, P.C., "Experimental Methods in Two-Phase Flow Studies", EPRI NP-118, 1975.

2. Lahey, R.T. Jr., "A Review of Selected Void Fraction and Phase Velocity Measurement Techniques", Short Course on Two-Phase Flow Measurements, Fluid Dynamics Institute, Dartmouth College, Hanover, Aug. 1978.

3. Hewitt, G.F., King, I., and Lovegrove, P.C., "Holdup and Pressure Drop Measurements in the Two-Phase Annular Flow of Air-Water Mixtures", UKAEA Report No. AERE-R3764, 1961

4. Roumy, R., "Structure of Two-Phase Air-Water Flows: Study of Average Void Fraction and Flow Patterns (In French)", CEA-R-3892, 1969.

5. Serizawa, A., "Fluid-Dynamic Characteristics of Two-Phase Flow", Inst. of Atomic Energy, Ph.D. Thesis, Kyoto University, 1974.

6. Schraub, F.A., Simpson R.I., and Janssen, E., "Two-Phase and Heat Transfer in Multirod Geometries", AECR and O Report GEAP-5739, 1969.

7. Colombo, A., Hassid, A., and Premoli, A., "Density Measurements in Heated Channels at High Pressure by Means of a Quick-Closing Valve Method", CISE Milan, Report No. CISE-R-232, 1967.

8. Agostini, G., Era, A., and Premoli, A., " Density Measurements of Steam-Water Mixtures Flowing in a Tubular Channel Under Adiabatic and Heated Conditions", CISE Milan, Report No. CISE-R-291, 1969.

9. Kemp, R.F., Morse, A.L., Wright, R.W., and Zivi, S.M., "Kinetic Studies of Heterogeneous Water Reactors", AEC Research and Dev. Report RWD-RL-167, 1959.

10. Cimorelli, L. and Premoli, A., "Measurement of Void Fraction with Impedance Gauge Technique", Energia Nucleare, 13, #1, 1966.

11. Kobori, T., Obata, T., Hagiya, A., and Terada, M., "Development of Void Meters for Transient Two Phase Flow", Proceedings of the CSNI Specialist Metting on Transient Two-Phase Flow, Toronto, 1976.

12. Delhaye, J.M., "Hot-Film Anemometry in Two-Phase Flow", ASME Symposium Volume, Two Phase Flow Instrumentation, 1969.

13. Miller, N. and Mitchie, R.F., "The Development of a Universal Probe for Measurement of Local Voidage in Liquid/ Gas Two Phase Flow Systems", ASME Symposium Volume, Two-Phase Flow Instrumentation, 1969.

14. Delhaye, J.M., "Local Measurements in Two-Phase Flow", Fluid Dynamic Measurements in the Industrial and Medical Environments, 1, Leicester University Press, 1972.

15. Barschdorff, D., Class, G., Loffel, R., and Reimann, J., "Mass Flow Measuring Techniques in Transient Two Phase Flow", Proceedings of the CSNI Specialist's Meeting on Transient Two-Phase Flow, Toronto, 1976.

16. Mayinger, F. and Panknin, W., "Holography in Heat and Mass Transfer", paper 1L3, Proceedings of the Fifth International Heat Transfer Conference, Tokyo, 1974.

17. Lockett, M.J. and Safekourdi, A.A., "Light Transmission Through Bubble Swarms", AIChE Journal, 23, No.3, pp. 395-398, 1977.

18. Wallis, G.B., One-Dimensional Two-Phase Flow, McGraw Hill, 1969.

19. Schrock, V.F., "Radiation Attenuation Techniques in Two-Phase Flow Measurements", ASME Symposium Volume, Two Phase Flow Instrumentation, 1969.

20. Petrick, M. and Swanson, B.S., "Radiation attenuation Method of Measuring Density of a Two-Phase Fluid", The Review of Scientific Instruments, 29, No.12, pp.1079-1085, 1958.

21. Bailey, R.V., Zmola, P.C., and Taylor, F.M., "Transport of Gases Through Liquid Gas Mixtures", ORNL-CF-55-12-118, 1955.

22. LeVert F.E. and Helminsky, E., "A Dual-Energy Method for Measuring Void Fractions in Flowing Mediums", Nuclear Technology, 19, pp 58-60, 1973.

23. Evangeliste R. and Lupoli, P., "The Void Fraction in an Annular Channel at Atmospheric Pressure", Int. Jnl. Heat Mass Transfer, 12, pp. 699-711, 1969.

24. Zakharova, E.A., Kolchugin, B.A., and Korniukhin, I.P., "Vapor Void-Fraction in Annular Channels at Separated and Joint Heat Supplied", 4th Int. Heat Transfer Conference, Paris, 5, Paper B5.5, 1970

25. Gustaffsson B. and Kjellen, B., "Two-Phase Flow in a 9 Rod Bundle with Inclined Power Distribution", European Two-Phase Flow Group Meeting, RISO Paper A5, Denmark, 1971.

26. Lassahn, G.D., "LOFT Three-Beam Densitometer Data Inter-
    pretation", TREE-NUREG-1111, 1977.

27. Heidrick, T.R., Saltvold, J.R., and Banerjee, S., "Appli-
    cation of a 3-Beam Gamma Densitometer to Two-Phase Flow
    Design and Density Measurements", AIChE Symposium Series-
    Nuclear, Solar and Process Heat Transfer, 73, 248-255, 1977.

28. Zielke, L.A., Howard, G.G., Currie, R.L., and Morgan, C.D.,
    "Rod Bundle Subchannel Void Fraction by Gamma Scattering",
    ANS Transactions, 22, 1972.

29. Kondic., N.N. and Lassahn, G.D., "Nonintrusive Density
    Distribution Measurement in Dynamic High Temperature
    Systems", Proceedings of the 24th International Instru-
    mentation Symposium, 1978.

30. Smith, A.V., "A Fast Response Multi-beam X-Ray Absorption
    Technique for Identifying Phase Distributions During
    Steam-Water Blowdowns", J. British Nuclear Energy Society,
    14, 1975.

31. Perkins, A.S. and Westwater, J.W., "Measurements of
    Bubbles Formed in Boiling Methanol", AIChE Journal, 2,
    pp 471-476, 1956.

32. Moss, R.A. and Kelly, A.J., "Neutron Radiographic Study
    of Limiting Planar Heat Pipe Performance", Int. J. Heat
    and Mass Transfer, 13, pp. 491-502, 1970.

33. Harms, A.A., Lo, S., and Hancox, W.T., "Measurement of
    Time-Averaged Voids by Neutron Diagnosis", J. Applied
    Physics, 42, 10, pp. 4080-4082, 1971.

34. Younis, M. H., "Void Disturbances in Two-Phase Flow
    Systems", Ph.D. Thesis, McMaster University, 1978.

35. Hancox, W.T., Forrest, C.F., and Harms, A.A., "Void
    Determination in Two-Phase Systems Employing Neutron
    Transmission", ASME Publication, Proceedings of AIChE-
    ASME Heat Transfer Conference, Denver, Colo, 1972.

36. Semel, S. and Helf, S., "Measurement of Low Concentrations
    of Moisture by Fast Neutron Moderation", Int. J. Applied
    Rad. and Isotopes, 20, 229-239, 1969.

37. Jackson, C.N. Jr., Alleman, R.T., and Spear, W.G.,
    "Neutron Densitometer for Measuring Void Fraction in
    Steam-Water Flow", Trans. Am. Nucl. Soc., 11, 1, 366-367,
    1968.

38. Sha, W.T. and Bonilla, C.F., "Out of Pile Steam Fraction
    Determination by Neutron-Beam Attenuation , Nucl. Appl.,
    1, 69-75, 1965.

39. Rousseau, J.C., Czerny, J., and Reigel, B., "Void Fraction Measurements During Blowdown by Neutron Absorption or Scattering Methods", Invited paper presented at OECD/NEA Specialists Meeting on Transient Two-Phase Flow, Toronto, 1976.

40. Banerjee, S., "Radiation Methods for Two-Phase Flow Measurements", Invited Lecture at USNRC Two-Phase Instrumentation Review Meeting, Washington, Jan. 1977.

41. McMaster Nuclear Reactor Annual Research Report, McMaster University, Hamilton, Ontario, Canada, Jan. 1978.

42. Price, W.J., Nuclear Radiation Detection, 2nd Ed., McGraw Hill, New York, 1964.

43. Allen, W.D., Neutron Detection, 1st Ed., Newnes, London, 1960.

44. Batchelor, R., Aves, R., and Skyrme, T.H.R., "Helium-3 Filled Proportional Counter for Neutron Spectroscopy", The Review of Scientific Instrument, Vol 26, No. 11, 1037-1047, 1955.

45. Herbst, L.J., Electronics for Nuclear Particle Analysis, Oxford University Press, 1970.

46. Cooper, B.E., Statistics For Experimentalists, Pergamon Press, Oxford, 1969